Atomic layer deposition of transition metal films and nanostructures for electronic and catalytic applications

James Maina, Andrea Merenda, Matthieu Weber, Jennifer Pringle, Mikhael Bechelany, Lachlan Hyde, Ludovic Dumée

Title

Atomic Layer Deposition of Transition Metal Films and Nanostructures for Electronic and Catalytic Applications

Authors

James W. Maina[1*], Andrea Merenda[1], Matthieu Weber[2], Jennifer M. Pringle[1], Mikhael Bechelany[2], Lachlan Hyde[3], Ludovic F. Dumée[1*]

Affiliations

1 Deakin University, Geelong, Institute for Frontier Materials, Waurn Ponds, 3216, Victoria, Australia

2 Institut Européen des Membranes, IEM-UMR 5635 ENSCM, UM, CNRS, Université de Montpellier, Place Eugène Bataillon, 34095 Montpellier Cedex 5, France.

3 Swinburne University of Technology, John Street, Hawthorn 3122, Victoria Australia

*Corresponding authors:

Dr. James Maina j.maina@deakin.edu.au +61415411649

Dr. Ludovic Dumee ludovic.dumee@deakin.edu.au +61410131312

Abstract

Atomic Layer Deposition (ALD) has emerged as the technique of choice in the microelectronics industry, owing to its self-limiting nature, that allows conformal film deposition in highly confined spaces. However, while the ALD of metal oxide has developed dramatically over the past decade, ALD of pure metal, particularly the transition metals has been developing at a very slow pace. This article reviews the latest development in the ALD of pure transition metals and alloys, for electronic and catalytic applications. In particular, the article analyzes how different factors, such as the substrate properties, deposition conditions, precursor and co-reactant properties, influence the deposition of the metal films and nanostructures, as well as the emerging applications of the ALD derived transition metal nanostructures. The challenges facing the field are highlighted, and suggestions are made for future research directions.

Keywords

Atomic layer deposition (ALD), transition metals, nanostructures, electronic applications, catalytic applications

1. Introduction

Atomic layer deposition (ALD) is a surface-controlled technique that allows the deposition of ultra-thin films one atomic layer at a time. [1] ALD utilizes self-limiting surface reactions between gaseous phase chemical precursors and chemically active sites on a substrate surface, enabling precise control over the film thickness, depending on the number of deposition cycles. The technique is also highly conformal, enabling deposition in highly confined spaces with ultra-high aspect ratio higher than 2000:1.[2-3] Consequently, ALD has recently attracted attention for the development of highly controlled nanostructures not only in the microelectronic field but also in sensing[4] photovoltaics,[5] membranes[6] and catalysis applications.[7-10].

The advancement in the ALD of metals has been driven primarily by the increased demand for miniaturized and hence more portable and energy-efficient devices in the electronic industry.[11-12] Copper, for example, is used as the primary interconnect material in the integrated circuits and is applied through electroplating on trenches and vias across the surface of insulating substrates.[13] The electroplating requires a thin and uniform seed layer, which is typically deposited using Physical Vapor Deposition (PVD). However, as the trenches and vias shrink in size, the high level of film conformity required is not achievable by PVD, due to limited diffusion capability of the vaporized film precursors across high aspect ratio materials.[14] In contrast, ALD may offer deposition of thin and highly conformal films across ultra-high aspect ratio nano-features, making it a promising alternative technique for metallic films deposition.

The ability to control material properties at an atomic scale, has also made ALD extremely promising for the design of nanoscale catalysts by addressing the challenges related to poor catalytic efficiency, limited reaction/product selectivity and catalyst deactivation.[7]

Nano-structured catalysts, for example, exhibit higher specific surface area and enhanced charge transfer kinetics leading to higher overall catalytic efficiency compared to their bulk counterparts.[7] The potential for ALD in facilitating the design of such metallic nanostructures has been demonstrated by using either specific templates or through selective area deposition.[15-17]

Furthermore, ALD can create sub-nanometer catalytic particles across substrates in a highly discrete manner,[18-20] which, in turn leads to a higher density of active sites compared to catalysts prepared using other conventional techniques, hence offering higher catalytic activity.[19] For successful deposition of such nanoparticles, the density of active site across the substrate should be relatively low and discretely spaced across the substrate, to allow for sufficient spacing between the individual seeding site. A high density of active sites will likely lead to intergrowth between the individual particles, ultimately leading to a continuous film. The potential for ALD in the deposition of single-atom catalyst has also been demonstrated, enabling 100% of the catalyst atoms to be located on the surface of the material, significantly boosting the number of active sites.[21-23] Such catalysts were shown to be highly selective towards particular reactions, compared to their particles counterpart, due to the absence of geometric and micro-structural defects, such as kinks and steps, typically present across nanoparticles. [22, 24] The highly discrete nature of ALD and the controlled spacing of deposited catalyst particles allows for high temperature catalytic reactions without inducing detrimental sintering of close-by particles.[7] ALD can also be used to apply an ultra-thin secondary layer on the surface not only to stabilize the catalyst, but also to tune the catalytic activity and selectivity towards a given reaction.[7, 25-26]

Although the ALD of metal oxides has been thoroughly investigated, the deposition of pure metals, particularly the transition metals, has grown at a very slow pace, hindering many potential applications.[13] The primary limitation has been the lack of sufficiently reactive metal

precursors that can react efficiently with common reducing agents.[13, 27] The ability to deposit a pure metal is related to the reduction potential, where a metal with a high reduction potential will have a lower energy barrier for deposition, while a metal with a lower reduction potential is more difficult to deposit in it's pure form.[13, 27] Consequently, noble metals such as Pt, Pd and Ru are relatively easier to deposit, due to their higher reduction potentials (1.19, 0.92 and 0.60 V, respectively), compared to transition metals, such as Cu, Ni, Co, and Fe , which have lower reduction potentials of 0.34, -0.25, -0.28 and -0.44 V, respectively. [27] A further challenge is the limited availability of precursors, combining high reactivity with sufficient thermal stability, to support self-limiting reactions at ALD temperatures.[13] The ALD of noble metals has been previously reviewed by several authors, [27-29] while the precursor chemistry and reaction mechanisms for the ALD of pure transition metals were reviewed by Knisley *et al.*[13] and Ramos *et al.*[27]. A general review in the application of ALD in the design of metals and metal oxide catalysts has also been previously published.[30]

This paper reviews the latest developments in the ALD of pure transition metals and alloys, for electronic and catalytic applications. In particular, the article differs from the aforementioned reviews, by conducting an in-depth analysis on how various parameters including substrate surface chemistry, deposition temperatures, precursor and co-reactant properties influence the deposition efficiency, as well as the key film properties, such as the continuity, roughness, purity and electrical conductivity. The review also highlights the emerging techniques for the fabrication of nanostructures such as templated and selective area ALD, and discusses the catalytic applications of ALD derived pure transition metal nanostructures. The current challenge hindering the advancement of the field are subsequently identified and the directions for future research are suggested.

2. Factors governing atomic layer deposition

The first step in ALD involves pulsing vapour of a metal precursor into the reaction chamber, where it adsorbs on the substrates and reacts with functional groups across the surface (Scheme 1).[1, 8] The first step relies on the reactivity of the precursor towards the functional groups available on the substrate surface, and it is critical to tune the surface chemistry to match a specific precursor.[13, 31-32] The excess precursor and the reaction by-products are subsequently purged with an inert gas, after which a co-reactant is pulsed into the chamber, to react with the terminal functional groups of the first precursor layer, while also introducing active sites for subsequent reactions. This step is again followed by a purge to remove excess co-reactants and by-products, after which the sequence can be repeated to obtain the desired thickness.[8]

The reliance of film nucleation on the substrate surface chemistry, makes it possible to selectively grow nanostructures by patterning the surface with functional groups that aid film nucleation, while deactivating other sites with passivating molecules such as the self-assembled monolayers.[33-34] In addition to the nature of surface chemistry, the surface energy of the substrate also has a big impact on film nucleation across the support. Metals that have a higher surface energy, such as Pt (surface energy 2.5 J/m^2) nucleate poorly on substrates that have a lower surface energy such as alumina (0.905 J/m^2) and silica (0.605 J/m^2)[35] leading to an 'island growth mode' and high surface roughness.[36-37] Using a substrate that has higher surface energy relative to the metal being deposited, on the other hand, can improve wettability, leading to a more homogenous film nucleation.

ALD can be classified into thermal atomic layer deposition and plasma enhanced atomic layer deposition (PEALD), also known as plasma-assisted atomic layer deposition (PA-ALD). Thermal ALD takes place at relatively higher temperatures, and it is important to establish the optimal deposition temperature range for each precursors, also known as 'ALD

temperature window' where the chemicals react in a self-limiting manner. Above the temperature window, the precursors start to decompose leading to the non-self-limiting chemical vapour deposition (CVD). The higher temperature may also lead to the desorption of precursors from the substrate surface, leading to a decrease in the deposition rate.[38] The metal precursor should also have higher vapour pressure to allow pulsing into the reactor at relatively lower precursor temperature, and have higher reactivity towards common reducing agents.[13] However, for some metals (e.g. Co), there are very limited precursors that meet these conditions, making thermal ALD ineffective. PEALD, can facilitate the deposition from such precursors, by employing plasma technology to convert elemental co-reactants into highly reactive radicals.[11] In addition, reactive ions and photons are generated during the process,[39] facilitating deposition from less reactive precursors, thus broadening the scope of materials that could be deposited through ALD. However, compared to thermal ALD, PEALD has limited conformity due to the short lifetime of the radicals, hindering conformal deposition in high aspect ratio structures[38] The use of plasma may also results in an increased level of impurities across metallic films, compromising their electrical properties, and may be destructive to some substrates. [11, 13]

3. ALD of pure transition metals

This section discusses the ALD of pure transition metals including Cu, Ni, Co and their alloys, by analyzing how different factors such as the substrate surface chemistry, deposition conditions, precursor and co-reactant properties, influence the final film properties.

3.1. ALD of Cu metal

Among other transition metals, copper is the most investigated for ALD, owing to its high electrical conductivity, making it useful for a wide range of electronic applications. [12-13, 27] Cu based catalysts are also widely used in industrially important catalytic reactions such as water gas shift reactions and methanol production, from the synthesis gas, and methanol steam reforming to produce hydrogen.[19, 40-41] Reaction selectivity towards a given product is governed not only by the composition but also the shape and morphology of the catalyst.[42] Kink and step sites, for example, have been shown to have higher selectivity towards hydrogenolysis reactions,[43] while nanoneedle shaped structures have been shown to exhibit higher activity towards CO_2 conversion, compared to other nanostructures, owing to their ability to generate localized electric field.[44] Therefore, the ability to control the composition and the nanostructural morphology at an atomic scale will enable highly selective catalyst for specific applications.[7] One challenge that hinders the application of nano-catalysts in high temperature catalytic reactions is the loss of activity due to sintering.[7] ALD enables discrete formation and deposition of Cu nano-catalysts across complex substrate architectures, enabling exposure to high temperature conditions without the loss of activity due to sintering.[7, 19] Although such nanostructures are also prone to deactivation via carbon poisoning, ALD could allow for the selective deposition of a secondary layer on the catalyst surface prior to the reaction, to suppress the carbon poisoning.[45]

3.1.1. Thermal ALD of Cu metal

Cu deposition by ALD can be achieved either indirectly by the ALD of CuO followed by reduction using formic acid or isopropanol,[13] or by direct deposition from appropriate Cu precursors and a reducing agent.[46] Direct deposition of Cu has been accomplished from a wide variety of Cu precursors including $Cu(tmhd)_2$ (4, tmhd =2,2,6,6-tetramethyl-3,5-heptanedionate), copper acetamidinates, copper chloride ($CuCl_2$), copper (II) hexafloroacetylacetonate hydrate ($Cu(hfac)_2$), Cu(I) β-diketiminate, copper dimethyl-2-propoxide ($Cu(dmap)_2$).[47-48] A copper acetamidinate precursor, for example, was prepared by a reaction between lithium N,N'-dialkylacetamidinate with copper chloride, and used for the deposition of Cu films at 280 ^oC, using molecular hydrogen as the reducing agent (Table 1, entry 1).[49] The deposition rate for Cu was found to be 0.5 Å/cycle, and the films were highly conformal, enabling highly continuous film in confined features with aspect ratios of 10:1. However, the films had a relatively high roughness of 6 nm for a 40 nm film thickness, which was attributed to low nucleation density across the SiO_2 substrate. Switching to ALD deposited Co substrate, resulted in an enhanced nucleation density, leading to a decrease in roughness from 6 to 2 nm. However, the electrical resistivity and the purity of the Cu films were not reported.

The deposition of Cu films from copper (I) amidinate precursors with the molecular hydrogen as the co-reactant was also reported (Table 1 entry 2-7).[31] The Cu precursor exhibits a melting point of 77 ^oC and was in a liquid state at the vaporization temperature of 90 – 120 ^oC. This state enabled a reproducible vapour pressure, leading to consistent film deposition even across very narrow holes with aspect ratio of 35:1. The study investigated deposition at temperatures ranging from 150 to 300 ^oC, where the film roughness was found to be dependent upon the nature of the substrate, precursor exposure time as well as deposition temperature. A relatively higher deposition rate ranging between 1.5 to 2 Å/cycle was found across SiO_2, Al_2O_3

and Si_3N_4, compared to the metallic substrates Ru, Co and Cu, which had lower deposition rates of 0.16, 0.28, and 0.15 Å/cycle, respectively (Table 1, entry 2 -7). However, the film deposited on SiO_2 had the highest roughness with large grain sizes of about 44 nm, which were separated from each other, while the film deposited on ALD Co surface had the smallest grain size and the most dense nucleation levels. The higher growth rate on the oxide surfaces was attributed to the rapid diffusion and agglomeration of copper and chemisorbed Cu precursors across the substrate surface to form large nuclei, and thereby freeing up additional active sites on the substrate to react with more Cu precursors. However, on metallic surfaces, the strong metallic bond between the deposited Cu and the metal substrate inhibited diffusion, which slowed the deposition rate since the active sites across the substrate were blocked by the deposited Cu film. This observation was supported by a scotch tape test, where films deposited on the oxide surface easily peeled off, while the one deposited on the metallic surface remained strongly adhered.

An increase in the precursors exposure time was found to result in an increased surface roughness, with Cu grain size increasing from 44 to 69 nm when the precursor exposure time was increased from 1 to 4 s.[31] Increasing the temperature was also shown to have a similar impact, with the roughness increasing from 29.4% at 150 ^{o}C, to 448.9% at 280 ^{o}C, relative to the film thickness. Rutherford Backscattering Spectroscopy (RBS) analysis found the films deposited at 190 ^{o}C, exhibited carbon impurities of 1 at.%, while films deposited at temperatures above 300 ^{o}C, had carbon impurities higher than 10 at.%, owing to thermal decomposition of the Cu precursor, implying the temperature was outside the ALD window. A 4 nm thick Cu film deposited on 2 nm Ru substrate at 185 ^{o}C had a resistivity of 2.9 μΩ-cm, which is close to that of bulk copper (1.68 μΩcm). The low resistivity was attributed to high purity, as well as the high density nucleation which led to smooth film morphology, thus reducing electron scattering.

A low temperature deposition process was also developed using Cu $(dmap)_2$ (dmap = 3-dimethylamino-2-butoxide) metal precursor and diethyl zinc (Et_2Zn) as the reducing agent (Table 1, entry 8).[15] During the first cycle, the $Cu(dmap)_2$ monolayer was adsorbed on the SiO_2 substrate through dipole-dipole interactions at temperature between 100 - 120 ^oC. The reaction between the $Cu(dmap)_2$ monolayer and Et_2Zn during the second cycle, led to the formation of Cu film with $Zn(dmap)_2$ and butane as the by-products. The self-limiting nature of the reaction was confirmed by varying the pulse time of the metal precursor from 0.5 to 10 s, where the film thickness was found to be saturated when the dose for $Cu(dmap)_2$ exceeded 2 s. In the case of Et_2Zn, the growth rate plateaued when pulse time exceeded 0.5 s. The growth of the Cu film was found to be linear in respect to the number of deposition cycles, with a growth rate of 0.2 Å/cycle. X-ray Photoelectron Spectroscopy (XPS) analysis confirmed that the films deposited between 100 – 120 ^oC were pure copper metal based on Cu(2p) and Cu(LMM) (LMM = transition between inner shells L and M). However, when the temperature was increased to 130 ^oC, Zn peaks were detected, with intensity increasing as the deposition temperature was increased, implying the decomposition of $Zn(dmap)_2$ and Et_2Zn at temperature above 120 ^oC. Zn contamination was also found in films deposited at temperatures below 100 ^oC in addition to a decreased deposition rate, which could imply incomplete evaporation of the $Zn(dmap)_2$ by-products. The films exhibited a low electrical resistivity of 2.75 μΩcm, which is an indication of high quality Cu films.

Selective deposition was also demonstrated by using octadecylsiloxane self-assembled monolayers (OTS-SAMs), applied using a master mould containing 3.1 μm wide lines separated by 2.7 μm spaces (Figure 1 a). ALD across the patterned surface resulted in deposition only in the areas not covered with OTS-SAMs, resulting in the production of high purity Cu lines matching the dimensions of the mould (Figure 1 b). The exposed Si sections exhibited polar silanol groups, which interacted favourably with the ALD precursors thus

promoting adsorption of the metal site. OTS-SAMs coated regions, on the other hand, are non-polar, which limits the interaction with the ALD precursors.

The potential for high selectivity ALD for the fabrication of complex nanostructures was also demonstrated, by using a nanoporous polycarbonate membrane as a template during the ALD. The PC membrane exhibited narrow pore size distributions at around 150 nm and the surface was passivated with OTS-SAMs, to allow deposition only within the surface of the pores and not across the outer surfaces of the membrane. The deposition resulted in the formation of Cu nanotubes with wall thickness of 18 nm and length of 12 μm (Figure 1 c, d), post dissolution of the polymer template with chloroform. The length of the nanotubes corresponded to the templates thickness, confirming the excellent conformity of the deposition process.

In separate studies, the selective deposition of Cu across Pd nanostructures was also demonstrated (Table 1, entry 9). [17] The Pd nanostructures were fabricated using electron beam lithography on oxidised Si substrate, and exhibited a size ranging between 250 nm and 5 μm. The ALD was carried from $Cu(thd)_2$ with H_2 as the reducing agent, where the optimal deposition temperature was found to be between 210 - 250 ^{o}C. The deposition at 210 ^{o}C produced Cu films selectively across the Pd nanostructures, with a film thickness greater than 55 nm obtained after 1,500 cycles, corresponding to deposition rate of about 0.37 Å/cycle. After 1,000 cycles, the large micron-sized patterns became larger, with an increased roughness on the edges, but the overall triangular shape remained the same. However, for smaller triangular patterns, with size of 250 nm base and height, the initial smooth pattern became lumpy and uneven, while the sharp defined edges became rounded, distorting the original triangular shape. The loss of the conformity was attributed to the evolution of grain structure during the nucleation, where surface diffusion led to the growth of grains, with size approaching that of the nanostructures. Although the deposition at lower temperature would be

expected to improve the conformity by suppressing surface diffusion, the deposition rate was too low, with no continuous film obtained at temperatures below 190 ^{o}C.

A three-sequence Cu deposition method involving Cu $(dmap)_2$, formic acid and hydrazine has also been developed.[47] The initial step involved reacting the Cu precursor with formic acid, to form copper (II) formate, which was subsequently reduced to copper film after the exposure to hydrazine (Table 1, entry 10). The deposition was carried out at 120 ^{o}C on a Si substrate, and the impact of each precursor on the film growth rate was investigated by varying the number of cycles and the length of each precursor pulse. The impact of deposition temperature was investigated at pulse lengths of 3.0, 0.2, and 0.2 s for the Cu precursor, formic acid and hydrazine respectively, with a purge length of 5.0 s and 1000 deposition cycles. The study revealed a constant deposition rate of 0.47 to 0.50 Å/cycle at temperatures between 100 to 170 ^{o}C, while lower deposition rates were observed at 80, 180 and 200 ^{o}C. The films exhibited low roughness, with 50 nm thick film exhibiting root mean square (RMS) surface roughness of 3.5 nm. Films deposited at 100, 120 and 140 ^{o}C exhibited a resistivity in the range of 9.6 – 16.4 μΩcm at 20 ^{o}C, which was comparable to that of 40 – 50 nm thick Cu films obtained via sputtering (resistivity of 6-8 μΩcm). Based on time of flight elastic recoil detection analysis (ToF-ERDA), the Cu purity ranged from 95.9-98.8%, with the films deposited at 100 ^{o}C, having the highest purity, while those deposited at 180 ^{o}C had the lowest purity owing to the self-decomposition of the precursors at higher temperature.

In a separate study, the of use of tertiary butyl hydrazine (TBH) as the reducing agent, facilitated the deposition of Cu films from the $Cu(dmap)_2$, without the need of the formic acid (Table 1, entry 11).[10] The self-limiting nature of the process was demonstrated at 120 ^{o}C, where a growth rate of 0.17 Å was detected within the first 125 – 1,000 cycles. However, after the surface had been completely covered by the film, the rate of deposition reduced to 0.05 Å/cycle. Compositional analysis using time of ToF-ERDA revealed a 54 nm films had high purity of

99.4 at.%, which translated to a low electrical resistivity of 1.9 μΩcm, among the lowest reported so far for Cu ALD films. The films could be deposited on hydrogen terminated Si, glass, alumina, TiN as well as Ru substrates.

The deposition of Cu films from copper acetyl acetonate ($Cu(acac)_2$), water and hydroquinone (HQ) has also been demonstrated, at temperatures ranging from 160 to 250 ^oC (Table 1, entry 12).[12] The deposition consisted of the following pulse time sequence; 3 s $Cu(acac)_2$, 4 s N_2, 3 s H_2O, 4 s N_2, 2 s HQ, and 3 s N_2. The ALD window was found to be between 210 to 250 ^oC, where exposure times of 3 and 4 s were long enough for self-saturating surface reactions, enabling constant deposition rate of 2 Å/cycle, which is higher than most of the previously reported ALDs of Cu films. In the first stage the $Cu(acac)_2$ reacts with H_2O to form Cu_2O. During the second stage, the HQ is oxidized on the surface to benzoquinone, producing H_2 that can reduce the copper oxide to metallic copper. However, based on simulation studies $Cu(acac)_2$ may also undergo successive dissociation on copper surface to form pure copper,[50] which could also have contributed to the higher deposition rate. The films had resistivity of 2 - 5 μΩcm, which was close to that of bulk copper.

The ability to form templated metal nanostructures offers tremendous potential in catalysis, as it could be employed to develop highly controlled nanostructure for optimal catalytic activity and selectivity.[9, 33] In the semiconductor industry, selective ALD has potential to reduce the cost of production by reducing lithography and etching steps as well as eliminating the need for expensive reagents. [17, 34, 51] Thermal ALD of Cu has been accomplished from various precursors at temperatures ranging from 100 to 300 ^oC. Copper dimethyl-2-propoxide ($Cu(dmap)_2$) precursor with diethylzinc (Et_2Zn) co-reactant afforded deposition at the lowest temperature of 100 to 120 ^oC, to achieve films with a resistivity of 2.75 μΩcm. The highest purity was achieved with $Cu(DMAP)_2$ combined with TBH, where a purity of 99.4 at.% was achieved, leading to low resistivity of 1.9 μΩcm. This is among the lowest

resistivity reported to date for Cu ALD, making the precursors promising for the deposition Cu interconnects on the integrated circuit.

3.1.2. Plasma enhanced ALD of Cu metal

Using plasma generated radicals instead of elemental reactants can enhance the ALD of metals, from otherwise unreactive precursors. Radical enhanced atomic layer deposition, for example, was used to facilitate the deposition of Cu on silicon and glass substrates, from $Cu(acac)_2$ with hydrogen radicals as the co-reactant, (Table 1 entry 13).[52] The self-limiting nature of the process was observed at 140 ^oC, where a constant growth rate of 0.18 Å/cycle was observed. The Cu films with a thickness of 25 nm had roughness in the range of 2 to 3 nm, with a resistivity of around 15 μΩcm. The higher resistivity was attributed to the fact that the film thickness was less than the mean-free path for electrons in copper (39 nm), leading to the scattering of electrons at the interface.

Plasma enhanced atomic layer deposition (PEALD) of Cu on tantalum (Ta) substrates has also been demonstrated from Bis(1-dimethylamino-2-methyl-2-butoxy)copper(MABOC) precursor with hydrogen plasma (Table 1, entry 14).[53] The Cu precursor is a liquid at room temperature, and could be introduced into the reaction chamber under its own vapour pressure, without the need of a carrier gas. The ALD temperature window was found between 100 to 180 ^oC, where a constant deposition rate of 0.65 Å/cycle was observed. The roughness was found to increase with the deposition temperature, where film deposited at 100 ^oC had a roughness of 1.59 nm, while films deposited at 150 and 180 ^oC had roughness of 2.25 and 2.65 nm, respectively. Films deposited at 150 ^oC had the lowest resistivity of 5.2 μΩcm, while films deposited at lower temperature had a relatively higher resistivity, with films deposited at 100 ^oC having a resistivity of around 7 μΩcm, owing to increased level of impurities. Above 150

^{o}C, the resistivity dramatically increased to about 13 μΩcm for the film deposited at 200 ^{o}C, due to increased surface roughness and film discontinuity.

Plasma enhanced deposition of Cu from $[Cu((Py)CHCOCF_3)_2]_2$ (Py = Pyridine) with hydrogen plasma was also reported (Table 1, entry 15).[54] The deposition was carried out at 190 ^{o}C, where a thickness of 80 - 100 nm was achieved after 500 cycles. The films deposited on quartz glass substrate (substrate RMS ~ 1 nm) had RMS roughness of 8.7 nm whereas that deposited on alumina (substrate RMS ~ 114.9 nm) had RMS value of 125.9 nm. XPS analysis detected up to 16 at.% oxygen impurities, in addition to minor carbon, nitrogen and fluorine impurities from ligand. Upon exposing the film to argon etching for 100 s, the C, N and F impurities were removed, but up to 9 at.% of O_2 impurities remained. The high content of oxygen impurities was attributed to the decomposition mechanism of the precursor, where part of oxygen might have remained bonded to the copper nuclei, which might be an indication of chemical vapour deposition. The films had a sheet resistance of 58 Ω/sq and 222 Ω/sq for films deposited on quartz and alumina respectively.

PEALD facilitates deposition from precursors that are not sufficiently reactive for thermal ALD, thus broadening the scope of the available precursors for atomic layer deposition. However, PEALD also leads to an increased level of impurities, due to plasma initiated precursor degradation, compromising the electrical properties of the metallic films. As summarized in Table 1, all Cu films deposited via PEALD exhibited higher resistivity compared to those deposited via thermal Cu ALD, owing to the higher level of impurities. In addition, some substrates may also be vulnerable to plasma destruction, limiting the number of substrates that can be used in the PEALD.

3.2. ALD of Ni metal

Similar to copper, nickel films have important electronic applications including magnetic random access memory, NiSi contact material, and metal insulators,[55-56] in addition to catalytic applications such as CO_2 conversion,[57], hydrogen evolution[58] and hydrogenolysis.[43]

3.2.1. Thermal ALD of Ni metal

Pure Ni films can be deposited directly from suitable precursors [13, 49] or indirectly, where NiO is first deposited by ALD, followed by the reduction with H_2 to form pure metal.[59],[60],[61] The indirect deposition of Ni films, for example, was demonstrated by first reacting bis(cyclopentadienyl)-nickel ($Ni(C_5H_5)_2$) with water at 165 ^oC to form NiO, which was subsequently reduced using H_2 plasma to form Ni metal.[61] The direct deposition of Ni films from Bis-Ni(II) with H_2 as the reducing agent, has been demonstrated at temperatures ranging between 200 to 300 ^oC (Table 1, entry 17).[62] The ALD window was found to be 200 - 250 ^oC, where the film deposition was found to be linearly dependent on the number of deposition cycle at 1.25 Å/cycle. At temperatures higher than 250 ^oC, the deposition rate increased with temperature, due to chemical vapour deposition (CVD). The films deposited at 220 ^oC had a resistance of 18.6 Ω/sq, which was comparable to resistance of films obtained by the conventional physical vapour deposition (PVD). However, a dramatic increase in the resistance was observed as deposition temperature was increased above 250 ^oC, owing to the degradation of surface morphology, as evidenced by AFM analysis, where surface roughness was found to increase with deposition temperature.

The ability to tailor the properties of Ni films deposited from nickel acetylacetonate ($Ni(acac)_2$, by changing the chain length of alcohol reducing agents was also demonstrated (Table 1, entry 18).[63] The deposition was carried at temperature range between 250 - 300 ^oC,

where the use of either ethanol or propanol as the reducing agent produced Ni_3C while the use of methanol produced Ni films with purity above 95 at.%, and carbon contamination of less than 5 at.%, located primarily on the surface. The metallic film with thickness between 15 - 60 nm, had resistivity of about 27 μΩ.cm, which was relatively higher compared that of bulk Ni (6.93 μΩcm). [56] A self-limiting growth was reached for $Ni(acac)_2$ pulse time of 2 s, where a constant deposition growth rate of about 0.065 Å/cycle was observed. Deposition at 300 ^oC produced the thermally stable cubic lattice structure, while lower temperature produced the metastable hexagonal structure.

A highly conformal and selective deposition of Ni films on Si and SiO_2 substrates, was also demonstrated from bis(dimethylamino-2-methyl-2-butoxo)nickel [$Ni(dmamb)_2$] metal precursor with NH_3 co-reactant (Table 1, entry 19).[64] The deposition was carried out at 300 ^oC, where a self-limiting growth rate of 0.64 Å/cycle was found at exposure time of >2 s. The films were of high quality with only small amount of oxygen and negligible amount of N and C impurities present, and with a resistivity of 25 μΩcm. The film deposition was also highly conformal, enabling deposition via holes having an aspect ratio of 5:1. This high conformity enabled the deposition of a uniform Ni film (20 nm thick) around Si nanowires, to form a Ni-Si core shell nanowire structures. Furthermore, selective deposition was demonstrated using an octadecyltrichlorosilane (OTS) self-assembled monolayer as the blocking layer. The OTS line patterns were applied on the substrate using photolithography, and consisted of 9 μm OTS coated regions and 3 μm uncoated regions. The Ni film only deposited on the OTS free regions, leading to the deposition of Ni line patterns with 3 μm width, separated by a distance of 9 μm, indicating a highly selective Ni film deposition.

The deposition of Ni films from bis(1,4-di-tert-butyl-1,3-diazadienyl)nickel with tert-butylamine co-reactant, on metal as well as on insulating substrates has also been investigated (Table 1, entry 20 – 21).[56] The deposition was investigated at temperature ranging between 160

to 220 ^{o}C, where the ALD window was found between 180 and 195 ^{o}C. The deposition rate for Ni deposition on Pt substrate at 180 ^{o}C was found to be 0.60 Å/cycle, and the resultant film had Ni purity higher than 97 %. The films also had low RMS values of < 2.5 %, for films with thickness of 18 nm and 60 nm. The deposition rate was different on Ru substrate, where no deposition was found within the first 150 cycles, after which a deposition rate of 0.12 Å/cycle was noted between 150 to 250 cycles. This increased to 0.18 Å/cycle at 500 cycles and to 0.44 Å/cycle at 1,000 cycles. The resistivity of a 60 nm thick film on Pt substrate was found to be 22.1 μΩcm, while that of 44 nm thick film on Ru substrate was found to be 30.6 μΩcm. For comparison, the resistivity for a reference nickel metal was 6.93 μΩcm. Generally, thinner films were found to have an increased resistance due to the intermixing between the substrates and the Ni layers. However, a continuous films could not be obtained on Cu substrate, while the attempt to deposit on insulating substrates (Si (100), SiO_2, Si-H and carbon doped oxides did not yield any films after 1,000 cycles, indicating selectivity towards the Pt and Ru metal substrates.

A high growth per cycle deposition process, has also been demonstrated, from N,N,N',N-tetramethyl-ethylenediamine) (bis(2,4-pentanedionato)) nickel II ($Ni(acac)_2$(tmeda)) precursor, with anhydrous hydrazine (N_2H_4) as the co-reactant (Table 1, entry 22).[55] The electron-rich metal precursor was developed by the modification of $Ni(acac)_2$ with N,N,N',N'-tetramethyl-ethylenediamine (tmeda). The deposition was carried out on SiO_2/Si(100) substrates, at temperature ranging between 220 to 300 ^{o}C, where the ALD window was found to be between 240 and 280 ^{o}C. The self-limiting nature of the process was demonstrated at 260 ^{o}C, where a constant deposition rate of 2.1 Å/cycle was achieved, demonstrating the highest Ni deposition rate/cycle reported to date. Control deposition experiments using the Ni precursor without the reducing agent at temperatures between 260 - 280 ^{o}C, found no film deposition, ruling out CVD driven deposition at this temperature range.

The Ni films were found to have an electrical resistivity of between 18.1 to 19.4 μΩcm, with the films deposited at 260 ^{o}C, having Ni purity of 95.1 at%, based on XPS analysis with the rest being C, N and O impurities. The films were also found to be smooth, with RMS roughness of 0.65 nm.

Among the various precursors for thermal ALD of Ni, the $(Ni(acac)_2(tmeda)$ precursor with hydrazine (N_2H_4) co-reactant appear to be the most promising, producing the highest reported deposition rate of 2.1 Å/cycle, and the lowest resistivity of 18.1 - 19.4 μΩcm (Table 1). However, this resistivity is almost three times higher than that of bulk Ni (6.93 μΩcm).[56] In addition, it appears more challenging to achieve high purity Ni ALD films as compared to copper, with the highest reported Ni film purity of 97% and most authors reporting purity below 95% (Table 1). This low purity explain the generally higher resistivity compared to the bulk Ni, and may be attributed to the lower reduction potential of Ni compared to Cu,[65] making it challenging to reduce Ni to its purest form.

3.2.2. Plasma enhanced ALD of Ni metal

The efficiency of hydrogen and NH_3 plasma in the deposition of Ni on Si substrates, using bis(dimethylamino-2-methyl-2-butoxo)nickel [$Ni(dmamb)_2$] precursor was investigated (Table 1, entry 23 - 24).[66] The study revealed a constant deposition rate of 2.0 and 0.8 Å/cycle for the NH_3 (APNi) and H_2 plasma (HPNi) enhanced films respectively, at 250 ^{o}C. However, at temperatures below 200 ^{o}C, the deposition rate using either of the plasma was the same at around 0.5 Å/cycle. XPS revealed a higher quantity of C impurities in HPNi compared to APNi, which resulted in higher a resistivity of 75 μΩcm compared to the 43 μΩcm obtained for the APNi.

The plasma enhanced deposition of 1D and 2D Ni nanostructures on highly ordered pyrolytic graphene (HOPG) substrates has also been demonstrated (Table 1, entry 25).[16] The study was carried out at 300 ^{o}C using Ni(dmamb)$_2$ metal precursor, with NH_3 gas or plasma. 1D nanowires were formed when NH_3 was used as the co-reactant, while the use of NH_3 plasma produced a continuous 2D film across the graphene surface. Within the first 100 cycles of deposition with the NH_3 gas co-reactant, the edges of the HOPG became decorated with Ni nanoparticles as shown in Figure 2 a. As the deposition continued, the particles became interconnected, leading to the formation of nanowire shaped structures.

The selective formation of nanowires across the edges of the HOPG was attributed to the higher reactivity of the edges compared to the basal planes. During the initial 200 cycles, the width of the nanowires grew at 2.07Å/cycle, but later decreased to 0.79 Å/cycle after the 200 cycles. This variation was attributed to the change in wettability on the HOPG, where wettability decreases as the deposition proceeds. The use of NH_3 plasma as the reactant, however, resulted in the formation of a continuous film across the HOPG, due to the higher reactivity of the NH_3 plasma which activated the basal planes of the HOPG, enabling uniform deposition across the surface.

Similar to Cu PEALD, higher resistivity values are observed in Ni PEALD as compared to thermal Ni film, with the resistivity ranging from 43 to 75 μΩcm, (Table 1). In addition to precursors, the type of plasma gas also plays critical role in the film deposition. For example, using NH_3 plasma instead of H_2 was shown to enhance the deposition rate by more than double from Ni(dmamb)$_2$ metal precursor, while also producing film with comparatively lower resistivity (Table 1 entry 23 – 24).[66] The higher deposition rate was attributed to the generation of NHx radicals which can participate in the ALD reactions to increase the deposition rate.

3.3. ALD of Co metal

Owing to its ferromagnetic properties, Co has a wide range of electronic applications including magnetic storage, magnetic field sensing and bio sensing.[67] However, it is relatively challenging to deposit pure Co compared to Cu and Ni because of its lower reduction potential, and most studies have employed PEALD for its deposition.

3.3.1. Thermal ALD of Co metal

The first ALD of Co was accomplished using cobalt bis(N,N'-diisopropylacetamidinate, with hydrogen gas as the reducing agent.[38] The deposition was carried out at 350 ^{o}C, where a deposition rate of 0.12 Å/cycle was observed. The Co was found to be highly conformal, enabling deposition on holes with high aspect ratio of up to 220:1. The Co films were found to be relatively smooth with an RMS roughness of 0.8 nm for a 15 nm thick film, while a 40 nm thick film was found to have a resistivity of 46 μΩcm. Although the film purity was not quantified, even very thin Co film with thickness of 0.8 nm were found to be electrically conductive, confirming a high quality metallic film.

A process for the deposition of Co from cobalt acetylacetonate ($Co(C_5H_7O_2)_2$, with hydrogen and silane as reducing agents was also developed (Table 1, entry 27 - 28). [68] The study investigated growth on a wide variety of substrates including, Ir, Ta, SiO_2, Si and fluorinated silica glass. While using H_2 as the reducing agent, Co deposition only occurred on Ir substrate, with no film growth observed on Ta, SiO_2 and Si substrates. The ALD window was found to be between 280 to 325 ^{o}C, where a deposition rate of 0.57 Å/cycle was observed. Substituting hydrogen with 0.5 % silane in argon as the reducing agent, enabled the deposition of Co films on Ta, SiO_2, Si, as well as the fluorinated silica glass (FSG), albeit at a lower

deposition rate compared to the Ir surface, with a maximum deposition rate of 0.38 Å/cycle. However, the work did not report the resistivity, roughness and the purity of the Co films.

3.3.2. Plasma enhanced ALD of Co metal

The PEALD of Co from dicobalt octacarbonyl ($Co_2CO)_8$) with hydrogen plasma was also investigated (Table 1, entry 29).[69] The study found the ALD window to be between 75 to 110 ^oC, where a constant deposition rate of 1.2 Å/cycle was recorded. However, the level of carbon and oxygen impurities in the films was found to be dependent upon the plasma power, where films deposited at plasma power of 50 W had oxygen and carbon impurities of 15 and 22 at.%, respectively, while films deposited at 300 W had oxygen and carbon contents of 2 and 15 at.% respectively. The higher level of impurities at a lower plasma power was attributed to incomplete decomposition of the Co-CO bonds, leaving residual precursors across the films. In a subsequent study, the team demonstrated that the higher level of impurities could be significantly reduced, by switching the metal precursor to cyclopentadienylcobalt dicarbonyl [$(CpCo(CO)_2$] (Table 1, entry 30).[70]

NH_3 plasma enhanced Co deposition was also demonstrated from cyclopentadienyl isopropyl acetamidinato-cobalt precursor, on SiO_2 and Si (001) substrates (Table 1, entry 31).[67] The deposition was carried out between 100 to 300 ^oC, where ALD window was found between 200 to 250 ^oC, with a deposition rate of 0.5 Å/cycle at 250 ^oC. However, XPS analysis found a high level of oxygen across the film, with up to 40 at.% on the surface, and around 10 at.% inside the Co film, which led to a relatively higher resistivity of 140 μΩcm.

The initial growth mechanism of Co films on Si substrates has also been investigated, using $CoCp_2$ precursor with NH_3 plasma at 300 ^oC (Table 1, entry 32).[71] The study found that the thickness of the film did not increase linearly with time, but increased rapidly during the

first 100 cycles to 1.4 Å/cycle, after which it decreased to 0.38 Å/cycle between 100 - 500 cycles. However, further investigation using synchrotron radiation X-ray reflectivity (SR-XRR) revealed that the relative density of the films increased abruptly for the first 10 cycles, and then it remained virtually unchanged up to 100 cycles. The density then increased between 100 - 500 cycles reaching a maximum of 0.7 relative to the bulk value of 8.9 g/cm^3. SEM imaging also found that the morphology of the film deposited after the first 100 cycles were rough and discontinuous, while that grown after 300 and 500 cycles had a much smoother and more continuous morphology (Figure 3) . This variation in morphology was attributed to the agglomeration of Co atoms, leading to island growth of Co at the early stage. At the initial stage, the formation of Si-N layer was observed following the exposure of the substrate to the NH_3 plasma during the first 10 cycles, which may inhibit Co growth on the substrate. Therefore, between 10 - 100 cycles, Co grew preferentially on locations that were already coated with Co films during the first 100 cycles, while still exposed Si-N domains exhibited limited or no growth, leading to the island growth mode, with apparent higher deposition rate but high roughness and low density across the substrate.

The use of NH_3 and H_2 gases as well as their plasma in the deposition of Co from $Co(MeCp)_2$ was also investigated, where only NH_3 plasma was found to beeffective in facilitating the deposition of Co across Si and SiO_2 substrates (Table 1, entry 33).[72] The deposition was investigated at temperature range between 100 to 350 ^oC, where similar deposition rates of between 0.4 to 0.6 Å/cycle were observed at temperature between 200 - 350 ^oC. However, the deposition rate increased at temperatures below 200 ^oC, with the highest deposition rate of 1.9 Å/cycle recorded at 100 ^oC. However, the samples prepared at lower temperature had a significantly higher level impurities with over 10% carbon and 5 % nitrogen impurities. This corresponded to an increase in electrical resistivity, with samples deposited at 100 ^oC having a resistivity of 8,500 μΩcm, compared to 31 μΩcm for samples deposited at

350 ^{o}C. The higher deposition rate at lower temperature was therefore attributed to the incomplete release of the organic metal precursors, leading to an increased level of impurities, and high resistivity.

Very recently, a PEALD process for the Co from bis(ethylcyclopentadienyl) cobalt $Co(EtCp)_2$ with NH_3 plasma has also been reported (Table 1, entry 34).[73] The study found the ALD window to be between 125 and 225 ^{o}C, where a constant deposition of about 0.073Å/cycle was observed, at pulse saturation times of 2 s and 20s for $Co(EtCp)_2$ and NH_3 plasma, respectively. However, the Co films exhibited low purity, with films deposited at 175 ^{o}C, having Co content of only 45%, even after 6 min etching to remove surface contaminants, with the rest being composed of 32% C, 18% N and 5% O. The higher content of C was attributed to the incomplete removal of the EtCp ligands, while the presence of O was attributed to oxygen contamination from the reaction chamber, with N contamination likely to have originated from NH_3 plasma. All the films were found to be smooth with RMS value of approximately 0.3 nm, but with a high resistivity of 117 μΩcm, owing to the low purity.

The ALD of Co has been accomplished primarily using PEALD. However, the resistivity was significantly high, ranging from 31 to 140 μΩcm (Table 1), compared to that of bulk Co, which has resistivity of 5.6 μΩcm.[74] This trend is consistent across Cu and Ni films, highlighting the limitations of PEALD in applications where high electrical conductivity is critical. However, the incorporation of N and C species within the metallic materials during PEALD, could potentially be harnessed for catalytic applications, since such dopants are known to result in enhanced catalytic activity.[75-76]

3.4. ALD of other transition metals

The deposition of transition metals with reduction potentials lower than -0.28 V (e.g. Fe, Mn, Ti and Cr) has been extremely limited, since they require a very strong reducing agent

to form a pure metal.[13, 77] As a result, ALD of most transition metals, including V, Zr, and Hf, has not yet been reported.

3.4.1. Thermal ALD of Mo, Fe, Cr and Ti

The deposition of molybdenum films from $MoCl_5$ and Zn was investigated at temperature range between 400 - 500 ºC (Table 1, entry 35).[78] The $MoCl_5$ was evaporated at 90 ºC, while Zn was evaporated at 390 ºC. A deposition rate of 0.8 Å/cycle was found at 420 ºC, but with Zn impurities of up to 2 at.%. The Zn impurities could be reduced to less than 1 at.% by increasing the purge time from 0.5 s to around 3 s, but the deposition rate also decreased to 0.4 Å/cycle. The Zn impurities was also found to promote oxide impurities on the surface with samples prepared with a purge time of 0.5 s containing about 30 at.% in its outermost half, while those prepared with purge time of 3 s had a very low oxygen content, implying the presence of residue Zn in the film may have promoted oxidation upon exposure to air. The resistivity of the film was also found to be dependent upon the Zn content, with samples having Zn content of less than 1 at.% having the lowest resistivity of 15 μΩcm with samples having Zn content higher than 2 at.% having resistivity higher than 25 μΩcm. However, it was critical to keep Zn and $MoCl_2$ pulse as short as possible, to limit Zn contamination on the film, as well as to prevent the $MoCl_2$ precursor from etching the already deposited film. These challenges also made it impossible to achieve the self-limiting reactions using the precursors.

The deposition of Fe films from iron bis(N,N'-diisopropylacetamidinate) with elemental hydrogen co-reactant was also reported (Table 1, entry 36).[49] The deposition was carried out at 250 ºC, where a growth rate of 0.08 Å/cycle was reported. The quality of the metallic film was confirmed by X-ray Photoelectron Spectroscopy (XPS) and Rutherford Backscattering Spectroscopy (RBS), though the actual purity of the film was not reported. The

Fe film exhibited the shiny metallic appearance, and were ferromagnetic, indicating the deposition of the metallic Fe.

New precursors for the deposition of transition metals including, Cu, Ni, Co, Fe, Mn and Cr, were also prepared by reacting MCl_2 with amino alkoxide salts (Table 1, entry 37).[77] The deposition of Ni, Co, Fe, Cr was carried out from $M(RR'COCNtBu)_2$ precursor while Mn was deposited from $[Mn(RR'COCNtBu)_2]_2$, all with borane dimethylamine ($BH_3(NHMe_2)$) as the reducing agent. The study investigated deposition across a wide variety of substrates including Ru, Pd, Pt SiO_2 and SiH. However, deposition was only accomplished on Ru substrate, and after applying a nucleation process, involving the deposition of 50 cycles. The films deposition rates per cycle were found to be 0.07 (Fe), 0.1 (Mn) 0.08 (Cr) 0.09 (Ni) and 0.07 Å Co. A detailed study for the deposition of Cr, found ALD temperature window between 170 and 185 ^oC, where a constant film deposition was found at the rate of 0.08 Å/cycle. However, the film thickness growth plateaued after the 1000 cycles, implying a possible catalytic role of Ru substrate in activating the reducing agent, which might stop after the active sites on the substrate are blocked by Cr. XPS analysis detected Cr 2P with binding energy corresponding to Cr_2O_3, but ion sputtering for 60 - 90 s led to the detection of Cr 2P with binding energy corresponding to pure Cr metal. AFM analysis confirmed films grown between 170 - 180 ^oC and RMS roughness 0.37 - 0.59, indicating a smooth surface.

The deposition of Ti films from titanium tetrachloride with 2-methyl-1,4-bis(trimethylsilyl)-2,5-cyclohexadiene (**1**) or 1,4-bis(trimethylsilyl)-1,4-dihydropyrazine co-reactant (**2**) has also been demonstrated (Table 1, entry 38).[79]The studies with **1** as the reducing agent found ALD window between 110 to 250 ^oC, where a similar growth rate of 0.06 Å/cycle was observed on SiO_2, Si, Pt and Ru surfaces. Films deposited at 140 ^oC, had a relatively smooth surface, with an 80 nm thick film exhibiting RMS roughness of 1.3 to 4.9 nm based on AFM measurements. XPS analysis found a high level of oxide on the surface, without any

indication of pure metal, even after ion sputtering for about 50 min, confirming a high level of oxidation on the sample surface. Measurements taken after 30 s found the films were not electrically conductive, confirming a rapid oxidation upon exposure to air. Up to 2.9 - 3 % carbon, 0.8 - 2.2 % Si, < 0.5 % N, and 1.8-2.3 % Cl impurities were also detected across the film even after 50 min scattering. Deposition with **2** as the reducing agent found similar properties, with the films exhibiting a high level of oxide close to the surface. The films prepared with the **2** as the reducing agent also had a higher level of impurities with 9-16% carbon and 50% nitrogen respectively, implying **1**, was a better reducing agent compared to **2.**

Owing to the high stability of their corresponding precursors, ALD of pure transition metals with low reduction potentials (below -0.28 V) has been limited. Few potential precursors were demonstrated, but the deposition rates were too low ranging between 0.08 to 0.8 Å/cycle (Table 1, entry 35 - 38), and the films had high content of impurities. Generally zerovalent state metal precursors have high volatility, enabling deposition under relatively mild conditions.[80] However, most of these precursors are less stable, limiting their application at higher deposition temperature. As oxidation state increase, the metal – organic ligand bond becomes increasingly strong, making it increasingly difficult to reduce it to pure metal. As a result, it is much difficult to deposit pure multivalent metals such as Ta, Ti, Mo and Al, as compared to divalent metals such as Cu and Ni. While the development of more stronger reducing agents is expected to improve the deposition of such metals, the role of substrates should not be underestimated. In addition to ensuring the surface chemistry of the substrate is right for the specific precursors, using catalytically active substrate may potentially facilitate the activation of the precursors and aid the pure metal deposition.[77]

3.5. Deposition of transition metal-based alloys/bimetallic structures

Alloying is an effective strategy for altering the electronic and catalytic properties of metal nanostructures, leading to improved performance.[25, 42, 81] By allowing an atomic scale control of alloy compositions, ALD may facilitate systematic studies to investigate the link between materials composition and their catalytic and electronic performance.[25] Metal alloys may be deposited by ALD through alternate deposition from various metal precursors, or by secondary deposition to form bimetallic structures. [82-84] Such bimetallic structure may intermix at the interface under ALD conditions or when exposed to higher annealing temperatures, to form homogenous alloy phases.[85] Combined with the templating technologies, ALD has potential to yield complex alloy nanostructures with enhanced catalytic, electronic and magnetic properties. However, alternate deposition from different precursors requires the precursor to have similar chemistry, to facilitate deposition at similar temperature range and using a common reducing agent, which is a major drawback, as such precursors are extremely scarce.[25, 77]

3.5.1. Thermal ALD

The alternate deposition strategy has also been employed in the deposition of NiFe alloy films for magnetic applications (Table 1, entry 39).[83]The process involved ALD of $Ni_xFe_{1-x}O_y$ followed by thermal reduction under hydrogen atmosphere to form pure Ni-Fe films. The $Ni_xFe_{1-x}O_y$ was deposited on SiO_2 substrates, via alternate exposure of nickelocene ($NiCp_2$) and Ferrocene ($FeCp_2$) with ozone (O_3) as the co-reactant. The precursors were applied in the following sequence; *m* pulses of $NiCP_2/O_3$ (*m* =1, 2 or 3), followed by n pulses of $FeCp_2/O_3$ cycles. The sequence was repeated until there were 2000 pulses for $NiCP_2/O_3$ and $FeCp_2/O_3$ cycles. The obtained films were subsequently reduced at 400 ^oC under hydrogen environment

to obtain pure Ni-Fe films. Energy dispersive X-ray spectroscopy (EDS) analysis found atomic ratios of Ni:Fe in films prepared with $NiCp_2$/$FeCp_2$ at a pulse ratio of 1 (*i.e.* m =1) to be 83:17, while those prepared with a pulse ratio of 2 and 3 had a Ni:Fe ratio of 89:11, and 92:8, respectively. However, the annealing step resulted in the development of holes across the film as the oxygen was liberated, which led to higher electrical resistivity of up to 10^{-6} Ωm, due to increased electron scattering by the holes. The team also demonstrated that the recipe could be used to fabricate Ni-Fe alloy nanostructures, by using a nano-porous alumina template (pore size = 60 nm) during the ALD. Upon dissolution of the template using chromic acid, nanotubes with an external diameter of 70 nm and a length of 8.7 μm were obtained, as illustrated by SEM images (Figure 4).

3.5.2. Plasma enhanced ALD

The deposition of Cu-Mn alloys on SiO_2 substrates, by the simultaneous pulsing of Cu and Mn metal precursors was demonstrated (Table 1, entry 40).[82] The alloy was deposited at 120 ºC from bis(1-dimethylamino-2-methyl-2-butoxy) copper (MABOC) and Mn(2,2,6,6-tetramethylheptane-3,5-dionate)$_3$ (Mn(thd)$_3$ with H_2 plasma as the common co-reactant. A deposition cycle consisted of pulsing the Cu and Mn metal precursors, purging with Ar gas, exposure to H_2 plasma, and a second purge with the Ar gas. A self-limiting growth of 0.65 Å/cycle was observed for precursors pulse times greater than 5 s, and hydrogen plasma exposure time greater than 1 s. The content of Mn in Cu could be varied from 0 to 10 at.% depending on the exposure time for the Mn precursor. The resistivity of the film increased with the increasing Mn content, where a 10 nm thick film of Cu, Cu-Mn (4.7 at.% Mn), and Cu-Mn (9.8 at.% Mn) were 5.67, 45.2 and 129.5 μΩcm, respectively. Upon annealing between 100 and 500 ºC, a decrease in the resistivity was observed across all the films, particularly those

with higher Mn content, with the alloy having Mn content of 9.8 at.% decreasing to about 60 μΩcm after annealing at 500 ^{o}C. This decrease was attributed to the out-diffusion of Mn atoms from the alloy, which are expected to segregate at the surface and the interfaces of the Cu-Mn alloy/SiO_2. The Mn segregation acts as a barrier (also referred to as a self-forming barrier), to inhibit the diffusion of Cu atoms onto the surrounding substrate. The diffusion of Cu in the integrated circuit is a significant problem, as it could compromise the properties of the surrounding dielectric materials.[73]

The deposition of Cu-Al alloy has also been demonstrated by alternate deposition from Cu and Al precursors at 150 ^{o}C (Table 1, entry 41).[86] Cu was deposited from bis(1-dimethyulamino-2-methyl-2-butoy) copper (MABOC) precursor with H_2 plasma while Al was deposited from trimethylaluminum (TMA) precursor, with a H_2 plasma. The Cu deposition cycle consisted of four pulses, involving 5 s for Cu metal precursor, 10 s for N_2 purge, 8 s for the H_2 plasma exposure, and 10 s for a second N_2 purge. Al deposition pulses consisted of 0.5 s for TMA, 5 s N_2 purge, 5 s H_2 plasma exposure and 10 s N_2 purge. Depending on the number of cycles from the Cu and Al precursors, the Al content in the alloy could be tuned from 0 to 15.6 at.% based on XPS analysis. The electrical resistivity was found to increase with Al content. Pure Cu had a resistivity of 28 μΩcm, while samples with Al content of around 15.6 at.% had a higher resistivity of almost 200 μΩcm, due to the electron scattering by Al atoms. Like the Cu-Mn alloy discussed above, annealing of the Cu-Al alloy resulted in a decrease in electrical resistance, with the alloy having an Al content of 4.6 at.% exhibiting the most significant decrease from about 85 to 66 μΩcm. The decrease was similarly attributed to the out-diffusion of Al atoms from the bulk, to segregate at Cu-Al/SiO_2 interfaces, where they form a self-forming barrier of AlO_x.

Application of ALD-derived transition metal films and nanostructures

4.1. Electronic applications

ALD has emerged as an enabling technology for the fabrication of microelectronic devices, such as memories devices, capacitors, transistors, and integrated circuits.[87,88] ALD grown metal nitride films, for example, find applications as electrodes for capacitors and as gate material for complementary metal-oxide-semiconductors (CMOS), as previously reviewed.[88] $BaTiO_3$ and $SrTiO_3$ ALD film are used as dielectric materials for capacitors in dynamic random access memories (DRAM), while Al_2O_3, ZrO_2 and HfO_2 ALD films are used as high dielectric constant gate oxide to reduce tunneling current in metal-oxide semiconductor field-effect transistor (MOSFET).[89] Tunneling current arise as electrons undesirably flow through thin insulator/dielectric materials, and is a major obstacle to the downscaling of electronic devices.[90] High dielectric constant metal oxide such as $Al2O_3$, ZrO_2 and HfO_2 exhibit higher resistance to tunneling current as compared to the conventional SiO_2 dielectrics, and ALD enables ultrathin yet high quality films of such materials to be deposited.[91] A schematic illustration of the cross-section of a MOSFET containing a 10 nm film of Al_2O_3 ALD is illustrated in Figure 5.

Among pure transition metals, copper is the most widely used owing to its high electrical conductivity. Almost all electronic devices rely on copper to interconnect different components across the microelectronic chips.[12] As the devices shrink in size, the joule heating arising as the current passes through the conductor becomes more pronounced, and it is critical to keep the resistivity as low as possible.[12, 92] ALD has played a key role in addressing this problem, by facilitating the deposition of a continuous film across the high aspect ratio vias and trenches on integrated circuits, thus affording conductivity similar to that of bulk copper.[13] However, to achieve the high film continuity and low resistivity required for the electronic applications, the chemistries for both the precursors and the substrate surface must be carefully controlled. The

precursors should be sufficiently stable at the deposition temperature to prevent the decomposition, which is likely to increase resistivity, while the substrate surface should have a high density of active site, to facilitate the nucleation of a continuous film. In addition, it is important to ensure the reactivity of the substrate surface functional groups match that of the precursor to ensure a complete reaction on the substrate surface, without introducing secondary contamination. For example, NHx functional groups have been shown to reduce film contamination as compared to -H functional groups, during the deposition of transition metal nitrides owing to their higher reactivity.[93]

However, owing to the higher diffusivity of Cu atoms, a barrier layer is typically required to prevent the diffusion of Cu to the underlying Si substrate. ALD of CuMg and CuAl alloys were proposed, where the ALD films were subjected to heat treatment, to promote the diffusion of Mg and Al ions to the interface, thus acting as the barrier layer between the Cu and the substrate.[82, 86] Potential future applications include the development of nanostructured Ni-Fe permalloys, used as magnetic core in electronic and electrical equipment.[83]

4.2. Catalytic applications

The ability to apply conformal catalyst coatings across complex nanostructures has made ALD an extremely promising technique for the design of nanocatalytic materials.[8] Coupled with the ability to control material composition at an atomic scale, these properties will be particularly useful in challenging catalytic reactions such as the catalytic conversion of CO_2, where reactions yields and selectivity are strongly influenced by both compositional and structural features.[42, 44] High curvature nanoneedle structures, for example, exhibit higher CO_2 conversion efficiency compared to nanorods or nanoparticles,[44] while Cu based electrocatalysts exhibit a higher selectivity for hydrocarbons compared to other metallic nanostructures.[42] ALD has the potential to allow such nanostructures through templated deposition, while precise

compositional control will enable single or bimetal nanostructures with enhanced product selectivity.[25]

ALD has been used to deposit Cu nanoparticles across SiO_2 substrates, and their performance in the catalytic conversion of CO_2 to CO demonstrated, and compared with that of particles formed through the conventional impregnation method.[19] The result found that the ALD nanoparticles had superior performance, with about 14 - 24 times higher turnover frequency (TOF) for the conversion of CO_2 to CO compared to those prepared through the impregnation method. The higher activity was attributed to the smaller size of the Cu nanoparticles deposited by ALD, which had an average size of 2.4 nm, compared to the 17.6 nm sized particles obtained by the impregnation method. The ALD particles were also highly dispersed, preventing the deactivation of catalyst due to sintering, after the high temperature hydrogenation reactions.

A controllable deposition of Ni nanoparticles, ranging in size from 2.4 to 3.3 nm across alumina substrates was also demonstrated, and their catalytic performance compared with similar particles obtained via the conventional impregnation method.[43] The ALD was carried from bis(cyclopentyldienyl)Ni with hydrogen as the reducing agent. The ALD particle size could be varied depending on the number of deposition cycles where 1 cycle produced 2.4 ± 0.1 nm while 5 cycles produced 3.3 ± 0.1 nm. Temperature programmed desorption analysis (CO-TPD) revealed that the ALD particles had up to 5 times higher number of active sites compared to similar particles prepared by the impregnation method. The ALD particles also had a higher density of step and kink sites, which led to higher selectivity for the hydrogenolysis of propylene to over 10 %, while the selectivity for the particles obtained by the impregnation method was below 0.4%.

Secondary ALD was also used to prepare Ni-Pt bimetallic catalysts (average size 9.4 ± 4.5 nm), and their performance in the dry reforming of methane was compared with that of a similar catalyst, prepared using the incipient wetness impregnation method.[84] The deposition process involved deposition of Ni nanoparticles, after which Pt was deposited on the Ni nanoparticles to form the bimetallic catalyst. Ni was deposited from bis(cyclopentadienyl)nickel ($NiCp_2$) with hydrogen gas at 300 ^oC. Pt, on the other hand, was deposited from trimethyl(methylcyclopentadienyl) platinum IV ($Me_3(MeCp)$ Pt) with hydrogen as the co reactant at 175 ^oC. The ALD-derived Ni-Pt catalyst was found to outperform similar catalyst prepared by the incipient wetness impregnation method for dry reforming of methane (DRM). The ALD bi-metallic nanoparticles exhibited a methane reforming rate of 122 $Lh^{-1}g_{metal}^{-1}$ which was twice the yield obtained by similar catalysts prepared by the impregnation method (Figure 6). The yield was also 3 and 4 times higher than that obtained with pure Ni and Pt, respectively, highlighting the synergistic impact of the bi-metal catalyst. The bimetallic catalysts were also found to coke less owing to a weaker C adsorption energy at the step edges and a higher C diffusion barrier on terraces. The coking resistance compared to the one prepared by the impregnation method, also suggest proper distribution of Pt across the bimetallic catalyst, which is known to inhibit coking.

Secondary deposition has also been employed in the synthesis of Ni-Cu bi-metallic nanoparticle catalysts across alumina substrates, for the hydrogenation of CO_2 to methanol.[81] The Ni catalyst was deposited from bis(cyclopentadienyl) nickel ($Ni(Cp)_2$) and O_3 at 150 ^oC for 50 cycles, followed by reduction with pure hydrogen at 500 ^oC. Catalytic studies found the ALD prepared catalyst had a methanol yield of 1.5 $mmolg^{-1}h^{-1}$, which was more than double that obtained by similar catalyst prepared by the impregnation method (0.7 $mmolg^{-1}h^{-1}$). The higher performance was attributed to the higher surface area of the ALD nanoparticles, providing more active sites for catalysis. The ALD catalysts were also found to have a better

alloy dispersion based on TEM analysis, which could contribute to the improved performance. However, no methanol generation was observed when only ALD deposited pure Ni was used, while Cu/AlO_3 produced 0.8 $mmolg^{-1}h^{-1}$, clearly demonstrating the synergistic role of the Ni-Cu alloy.

ALD metal nanostructures outperform similar structures prepared using other conventional methods in a wide range of important catalytic applications, owing to their higher uniformity, better dispersion across a substrate and higher density of active sites. The layer by layer deposition technique allows control over size, down to the sub-nanometer scale, significantly boosting the number of active sites.[22] Although such nanostructures are also vulnerable to deactivation by carbon deposits on the active sites, ALD has been demonstrated as an effective technique for the selective deposition of a secondary material to suppress the carbon poisoning.[45]

5. Conclusion and perspectives

This review has highlighted the latest developments in the ALD of pure transition metals films and nanostructures, by analysing various factors that govern a successful deposition. Among the transition metals, the deposition of Cu, Ni and Co is the most developed, while the deposition of other metals such as V, Zr, and Hf has not been reported to date. Although the biggest challenge is the lack of sufficiently reactive precursors, for the deposition of pure metals, a much deeper understanding on the performance of the currently existing precursors, with a wide variety of substrate chemistries and co-reactants, will aid the progress of the field. Precursors that appear unreactive with certain substrate/co-reactant combination may become reactive when exposed to different chemistries, and systematic studies are necessary to establish the optimal precursor/substrate/co-reactant combinations. Using substrates that have a higher surface energy relative to the metal being deposited, for example, will result in an improved wettability, leading to more continuous films.[36]

The application of ALD in the deposition of transition metal catalysts has also been highlighted, where higher activity was demonstrated across a wide variety of chemical reactions, owing to improved dispersibility, higher specific surface area, and a higher density of active site. Through templated or selective ALD, it is expected that complex nanostructures with improved charge transfer kinetics, and hence higher catalytic activity will be developed. Future work should therefore explore the potential for the templated or selective area deposition in developing high curvature nanostructures (e.g. nanoneedles, and nanospikes), which exhibit higher electrocatalytic activity compared to other nanostructures. The capability of ALD to deposit in highly confined spaces should also be exploited to develop and stabilize the highly active single-atom metal catalysts within porous materials.[24, 94] ALD should also facilitate the design of magnetic-alloy nanostructures, having enhanced magnetic properties, for use as magnetic core in electrical and electronic equipments.[83]

Table 1. Precursors, deposition conditions and film properties of ALD deposited transition metals

Entry	Metal	Precursors	Deposition temperature	Substrate	GPC (Å/cycle)	Purity	Resistivity	Ref.
1.	CuCu (Thermal)	Copper aceta-midinate with H_2	280 °C	SiO_2, Co/SiO_2	0.5	-	-	[49]
2.		Copper (I) amidinates with H_2	150 - 300 °C	SiO_2/Al_2O_3	1.90	> 90 %		[31]
3.				S_3N_4	1.5			
4.				WN	0.54			
5.				Ru	0.11		2.9 μΩcm	
6.				Co	0.4			
7.				Cu	0.5			
8.		Copper dimethyl-2-propoxide ($Cu(dmap)_2$) with diethylzinc (Et_2Zn)	100 - 120 °C	SiO_2	0.2	-	2.75 μΩcm	[15]
9.		$Cu(thd)_2$ with H_2	210 - 250 °C.	Pd	0.37	-	-	[17]
10.		Cu $(dmap)_2$ with formic acid and hydrazine	120 °C	Si	0.47 - 0.50	95.9 -98.8 %,	9.6 – 16.4 μΩcm	[47]
11.		Cu $(dmap)_2$ with tertiary butyl hydrazine (TBH)	120 °C	SiH, SiO_2, Al_2O_3, TiN and Ru	0.17	99.4 at.%,	1.9 μΩcm	[10]
12.		Copper (II) acetyl-acetonate $Cu(acac)_2$ with water and hydroquinone	210 - 250 °C		2		2-5 μΩcm	[12]
13.	Cu (PEALD)	$Cu(acac)_2$ with H_2 plasma	140 °C	Si, SiO_2	0.18	≤ 86 %	15 μΩcm	[52]
14.		Bis (1-dimethyl-amino- 2-methyl-2-butoxy) copper (MABOC) with H_2 plasma	100 - 180 °C	Ta	0.65	> 95%	5.2 μΩcm	[53]
15.		$[Cu((Py)CHCOCF_3)_2]_2$ (Py = Pyridine) with H_2 plasma	190 °C	Quartz		~84 at.%	58 Ω /sq	[54]
16.				Al_2O_3			222 Ω /sq	
17.	Ni (Thermal)	Bis-Ni(II) with H_2	200 - 250 °C	Si	1.25	~ 75 at.%	18.6 Ω/sq	[62]
18.		Nickel (II) acetylacetonate ($Ni(acac)_2$) with methanol	250 -300 °C		0.065	95 at.%,	27 μΩcm	[63]

Entry	Metal	Precursors	Deposition temperature	Substrate	GPC (Å/cycle)	Purity	Resistivity	Ref.
19.		Bis(dimethylamino-2-methyl-2-butoxo)nickel [$Ni(dmamb)_2$ with NH_3	300 °C,	Si	0.64 Å/cycle	-	25 μΩcm	[64]
20.	Ni (Thermal)	Bis(1,4-di-tert-butyl-1,3-diazadienyl)-nickel with tertbutylamine	180 - 195 °C	Pt	0.60	97 at.%,	22.1 μΩcm	[56]
21.				Ru	-	-	30.6 μΩcm	
22.		$(Ni(acac)_2(tmeda)$ with N_2H_4	240 - 280 °C	SiO2/Si	2.1	95.1	18.1 - 19.4 μΩcm	[55]
23.	Ni (PEALD)	$Ni(dmamb)_2$ with NH_3 plasma	250 °C	Si	2.0	-	43 μΩcm	[66]
24.		$Ni(dmamb)_2$ with H_2 plasma	250 °C	Si	0.8	-	75 μΩcm	[66]
25.		$Ni(dmamb)_2$ with NH_3 gas	300 °C	HOPG	2.07 (initial) 0.79 after 200 cycles	-		[16]
26.	Co (Thermal)	Cobalt Bis(N,N'-diisopropylacetamidinate with H_2	350	SiO_2,	0.12	-	46 μΩcm	[49]
27.		Cobalt acetylacetonate with H_2	280 - 325 °C	Ir	0.57	-	-	[68]
28.		Cobalt acetylacetonate with silane	280 - 325 °C	Ta, SiO_2, Si, FSG	≤ 0.38	-	-	[68]
29.	Co (PEALD)	$(Co_2CO)_8$) with H_2 plasma	75 - 110 °C	So	1.2	63 - 83%		[69]
30.		Cyclopentadienylcobalt dicarbonyl ($(CpCo(CO)_2$) with H_2 plasma	125 - 175 °C	Si	1.1	≥ 91%	-	[70]
31.		Cyclopentadienyl isopropyl acetamidinato-cobalt with NH_3 plasma	200 - 250 °C	Si and SiO_2	0.5	60 – 90 %	140 μΩcm	[67]
32.		Cobaltocene ($CoCp_2$) with NH_3 plasma	300	Si	~0.48	-	-	[71]
33.		$Co(MeCp)_2$ with NH_3 plasma	200 - 350 °C	Si and SiO_2	0.4-0.6	-	31 μΩcm	[72]
34.		Bis(ethylcyclopentadienyl) cobalt ($Co(EtCp)_2$) with NH_3 plasma	125 - 225 °C	Si	0.073	45 %	117 μΩcm	[73]
35.	Mo (Thermal)	$MoCl_5$ with Zn	400 - 500 °C.	SiO_2, Al_2O_3	0.8	≤ 70 %	15 μΩcm	[78]
36.	Fe (Thermal)	Iron bis(N,N'-diisopropylacetamidinate)	250 °C		0.08	-	-	[49]

Entry	Metal	Precursors	Deposition temperature	Substrate	GPC (Å/cycle)	Purity	Resistivity (μΩcm)	Ref.
37.	Cr (Thermal)	$Cr(RR'COCNtBu)_2$ with $BH_3(NHMe_2)$	170 - 185 °C	Ru	0.08	-	-	[77]
38.	Ti (Thermal)	titanium tetrachloride with 2-methyl-1,4-bis(trimethylsilyl)-2,5-cyclohexadiene	110 - 250 °	SiO_2, Si, Pt and Ru	0.06	-	-	[79]
39.	Ni-Fe alloy (Thermal)	Nickeloccene ($NiCp_2$) and ferrocene ($FeCp_2$) with ozone (O_3) and H_2	200	SiO_2	0.26	-	$10-6\ \Omega$ m	[83]
40.	Cu-Mn alloy (Plasma)	Bis(1-dimethylamino-2-methyl-2-butoxy)copper (MABOC) and $(Mn(thd)_3$ with H_2 plasma	120	SiO_2	0.65	-	5.67- 129.5 μΩcm	[82]
41.	Cu-Al alloy (Plasma)	MABOC and trimethylaluminum with H_2 plasma	150	SiO_2			28 - 200 μΩcm	[86]

Acknowledgment

Dr. James W. Maina would like to thank Deakin University for his Alfred Deakin Research Fellowship. Dr. Ludovic F. Dumee acknowledges the Australian Research Council for his Discovery Early Career Research Award (DECRA).

References

1. Johnson, R. W.; Hultqvist, A.; Bent, S. F., A brief review of atomic layer deposition: from fundamentals to applications. *Materials Today* **2014,** *17* (5), 236-246.
2. Dasgupta, N. P.; Meng, X.; Elam, J. W.; Martinson, A. B. F., Atomic Layer Deposition of Metal Sulfide Materials. *Accounts of Chemical Research* **2015,** *48* (2), 341-348.
3. Kia, A. M.; Haufe, N.; Esmaeili, S.; Mart, C.; Utriainen, M.; Puurunen, R. L.; Weinreich, W., ToF-SIMS 3D Analysis of Thin Films Deposited in High Aspect Ratio Structures via Atomic Layer Deposition and Chemical Vapor Deposition. *Nanomaterials* **2019,** *9* (7), 1035.
4. Graniel, O.; Weber, M.; Balme, S.; Miele, P.; Bechelany, M., Atomic layer deposition for biosensing applications. *Biosensors and Bioelectronics* **2018,** *122*, 147-159.
5. Schmidt, J.; Merkle, A.; Brendel, R.; Hoex, B.; de Sanden, M. C. M. v.; Kessels, W. M. M., Surface passivation of high-efficiency silicon solar cells by atomic-layer-deposited Al2O3. *Progress in Photovoltaics: Research and Applications* **2008,** *16* (6), 461-466.
6. Weber, M.; Julbe, A.; Ayral, A.; Miele, P.; Bechelany, M., Atomic Layer Deposition for Membranes: Basics, Challenges, and Opportunities. *Chemistry of Materials* **2018,** *30* (21), 7368-7390.
7. Asundi, A. S.; Raiford, J. A.; Bent, S. F., Opportunities for Atomic Layer Deposition in Emerging Energy Technologies. *ACS Energy Letters* **2019,** *4* (4), 908-925.
8. O'Neill, B. J.; Jackson, D. H.; Lee, J.; Canlas, C.; Stair, P. C.; Marshall, C. L.; Elam, J. W.; Kuech, T. F.; Dumesic, J. A.; Huber, G. W., Catalyst design with atomic layer deposition. *Acs Catalysis* **2015,** *5* (3), 1804-1825.
9. Cao, K.; Cai, J.; Liu, X.; Chen, R., Review Article: Catalysts design and synthesis via selective atomic layer deposition. *Journal of Vacuum Science & Technology A* **2018,** *36* (1), 010801.
10. Väyrynen, K.; Mizohata, K.; Räisänen, J.; Peeters, D.; Devi, A.; Ritala, M.; Leskelä, M., Low-Temperature Atomic Layer Deposition of Low-Resistivity Copper Thin Films Using Cu(dmap)2 and Tertiary Butyl Hydrazine. *Chemistry of Materials* **2017,** *29* (15), 6502-6510.
11. Knoops, H. C.; Faraz, T.; Arts, K.; Kessels, W. M., Status and prospects of plasma-assisted atomic layer deposition. *Journal of Vacuum Science & Technology A: Vacuum, Surfaces, and Films* **2019,** *37* (3), 030902.
12. Tripathi, T. S.; Karppinen, M., Efficient Process for Direct Atomic Layer Deposition of Metallic Cu Thin Films Based on an Organic Reductant. *Chemistry of Materials* **2017,** *29* (3), 1230-1235.
13. Knisley, T. J.; Kalutarage, L. C.; Winter, C. H., Precursors and chemistry for the atomic layer deposition of metallic first row transition metal films. *Coordination Chemistry Reviews* **2013,** *257* (23-24), 3222-3231.
14. He, W., ALD: atomic layer deposition, precise and conformal coating for better performance. *Handbook of Manufacturing Engineering and Technology* **2013**, 1-33.
15. Lee, B. H.; Hwang, J. K.; Nam, J. W.; Lee, S. U.; Kim, J. T.; Koo, S.-M.; Baunemann, A.; Fischer, R. A.; Sung, M. M., Low-Temperature Atomic Layer Deposition of Copper Metal Thin Films: Self-Limiting Surface Reaction of Copper Dimethylamino-2-propoxide with Diethylzinc. *Angewandte Chemie* **2009,** *121* (25), 4606-4609.
16. Ryu, S. W.; Yoon, J.; Moon, H.-S.; Shong, B.; Kim, H.; Lee, H.-B.-R., Atomic layer deposition of 1D and 2D nickel nanostructures on graphite. *Nanotechnology* **2017,** *28* (11), 115301.
17. Qi, J.; Zimmerman, D. T.; Weisel, G. J.; Willis, B. G., Nucleation and growth of copper selective-area atomic layer deposition on palladium nanostructures. *The Journal of Chemical Physics* **2017,** *147* (15), 154702.
18. Feng, H.; Libera, J. A.; Stair, P. C.; Miller, J. T.; Elam, J. W., Subnanometer Palladium Particles Synthesized by Atomic Layer Deposition. *ACS Catalysis* **2011,** *1* (6), 665-673.
19. Chen, C. S.; Lin, J. H.; You, J. H.; Chen, C. R., Properties of Cu(thd)2 as a Precursor to Prepare Cu/SiO2 Catalyst Using the Atomic Layer Epitaxy Technique. *Journal of the American Chemical Society* **2006,** *128* (50), 15950-15951.

20. Weber, M.; Collot, P.; El Gaddari, H.; Tingry, S.; Bechelany, M.; Holade, Y., Enhanced Catalytic Glycerol Oxidation Activity Enabled by Activated-Carbon-Supported Palladium Catalysts Prepared through Atomic Layer Deposition. *ChemElectroChem* **2018,** *5* (5), 743-747.
21. Sun, S.; Zhang, G.; Gauquelin, N.; Chen, N.; Zhou, J.; Yang, S.; Chen, W.; Meng, X.; Geng, D.; Banis, M. N.; Li, R.; Ye, S.; Knights, S.; Botton, G. A.; Sham, T.-K.; Sun, X., Single-atom Catalysis Using Pt/Graphene Achieved through Atomic Layer Deposition. *Sci Rep* **2013,** *3*, 1775.
22. Cheng, N.; Stambula, S.; Wang, D.; Banis, M. N.; Liu, J.; Riese, A.; Xiao, B.; Li, R.; Sham, T.-K.; Liu, L.-M.; Botton, G. A.; Sun, X., Platinum single-atom and cluster catalysis of the hydrogen evolution reaction. *Nature Communications* **2016,** *7*, 13638.
23. Zhang, L.; Banis, M. N.; Sun, X., Single-atom catalysts by the atomic layer deposition technique. *National Science Review* **2018,** *5* (5), 628-630.
24. Kim, J.; Kim, H.-E.; Lee, H., Single-Atom Catalysts of Precious Metals for Electrochemical Reactions. *ChemSusChem* **2018,** *11* (1), 104-113.
25. Lu, J.; Low, K.-B.; Lei, Y.; Libera, J. A.; Nicholls, A.; Stair, P. C.; Elam, J. W., Toward atomically-precise synthesis of supported bimetallic nanoparticles using atomic layer deposition. *Nature Communications* **2014,** *5*, 3264.
26. Cheng, N.; Shao, Y.; Liu, J.; Sun, X., Electrocatalysts by atomic layer deposition for fuel cell applications. *Nano Energy* **2016,** *29*, 220-242.
27. Ramos, K. B.; Saly, M. J.; Chabal, Y. J., Precursor design and reaction mechanisms for the atomic layer deposition of metal films. *Coordination chemistry reviews* **2013,** *257* (23-24), 3271-3281.
28. Hämäläinen, J.; Ritala, M.; Leskelä, M., Atomic Layer Deposition of Noble Metals and Their Oxides. *Chemistry of Materials* **2014,** *26* (1), 786-801.
29. Weber, M. J.; Mackus, A. J. M.; Verheijen, M. A.; van der Marel, C.; Kessels, W. M. M., Supported Core/Shell Bimetallic Nanoparticles Synthesis by Atomic Layer Deposition. *Chemistry of Materials* **2012,** *24* (15), 2973-2977.
30. Lu, J.; Elam, J. W.; Stair, P. C., Atomic layer deposition—Sequential self-limiting surface reactions for advanced catalyst "bottom-up" synthesis. *Surface Science Reports* **2016,** *71* (2), 410-472.
31. Li, Z.; Rahtu, A.; Gordon, R. G., Atomic layer deposition of ultrathin copper metal films from a liquid copper (I) amidinate precursor. *Journal of The Electrochemical Society* **2006,** *153* (11), C787-C794.
32. Miikkulainen, V.; Leskelä, M.; Ritala, M.; Puurunen, R. L., Crystallinity of inorganic films grown by atomic layer deposition: Overview and general trends. *Journal of Applied Physics* **2013,** *113* (2), 021301.
33. Mackus, A. J. M.; Bol, A. A.; Kessels, W. M. M., The use of atomic layer deposition in advanced nanopatterning. *Nanoscale* **2014,** *6* (19), 10941-10960.
34. Mackus, A. J. M.; Merkx, M. J. M.; Kessels, W. M. M., From the Bottom-Up: Toward Area-Selective Atomic Layer Deposition with High Selectivity. *Chemistry of Materials* **2019,** *31* (1), 2-12.
35. Overbury, S. H.; Bertrand, P. A.; Somorjai, G. A., Surface composition of binary systems. Prediction of surface phase diagrams of solid solutions. *Chemical Reviews* **1975,** *75* (5), 547-560.
36. Clancey, J. W.; Cavanagh, A. S.; Kukreja, R. S.; Kongkanand, A.; George, S. M., Atomic layer deposition of ultrathin platinum films on tungsten atomic layer deposition adhesion layers: Application to high surface area substrates. *Journal of Vacuum Science & Technology A* **2015,** *33* (1), 01A130.
37. <Activation of HKUST-1 improves CO2 adsorption Liang et al 2009.pdf>.
38. George, S. M., Atomic Layer Deposition: An Overview. *Chemical Reviews* **2010,** *110* (1), 111-131.
39. Profijt, H. B.; Potts, S. E.; Sanden, M. C. M. v. d.; Kessels, W. M. M., Plasma-Assisted Atomic Layer Deposition: Basics, Opportunities, and Challenges. *Journal of Vacuum Science & Technology A* **2011,** *29* (5), 050801.

40. Xu, X.; Shuai, K.; Xu, B., Review on copper and palladium based catalysts for methanol steam reforming to produce hydrogen. *Catalysts* **2017,** *7* (6), 183.
41. Gokhale, A. A.; Dumesic, J. A.; Mavrikakis, M., On the mechanism of low-temperature water gas shift reaction on copper. *Journal of the American Chemical Society* **2008,** *130* (4), 1402-1414.
42. Kim, D.; Resasco, J.; Yu, Y.; Asiri, A. M.; Yang, P., Synergistic geometric and electronic effects for electrochemical reduction of carbon dioxide using gold–copper bimetallic nanoparticles. *Nat Commun* **2014,** *5*.
43. Gould, T. D.; Lubers, A. M.; Neltner, B. T.; Carrier, J. V.; Weimer, A. W.; Falconer, J. L.; Will Medlin, J., Synthesis of supported Ni catalysts by atomic layer deposition. *Journal of Catalysis* **2013,** *303*, 9-15.
44. Liu, M.; Pang, Y.; Zhang, B.; De Luna, P.; Voznyy, O.; Xu, J.; Zheng, X.; Dinh, C. T.; Fan, F.; Cao, C.; de Arquer, F. P. G.; Safaei, T. S.; Mepham, A.; Klinkova, A.; Kumacheva, E.; Filleter, T.; Sinton, D.; Kelley, S. O.; Sargent, E. H., Enhanced electrocatalytic CO2 reduction via field-induced reagent concentration. *Nature* **2016,** *537*, 382.
45. Ding, L.; Yi, H.; Zhang, W.; You, R.; Cao, T.; Yang, J.; Lu, J.; Huang, W., Activating Edge Sites on Pd Catalysts for Selective Hydrogenation of Acetylene via Selective Ga2O3 Decoration. *ACS Catalysis* **2016,** *6* (6), 3700-3707.
46. Huo, J.; Solanki, R.; McAndrew, J., Characteristics of copper films produced via atomic layer deposition. *Journal of Materials Research* **2002,** *17* (9), 2394-2398.
47. Knisley, T. J.; Ariyasena, T. C.; Sajavaara, T.; Saly, M. J.; Winter, C. H., Low Temperature Growth of High Purity, Low Resistivity Copper Films by Atomic Layer Deposition. *Chemistry of Materials* **2011,** *23* (20), 4417-4419.
48. Törndahl, T.; Ottosson, M.; Carlsson, J.-O., Growth of copper metal by atomic layer deposition using copper(I) chloride, water and hydrogen as precursors. *Thin Solid Films* **2004,** *458* (1), 129-136.
49. Lim, B. S.; Rahtu, A.; Gordon, R. G., Atomic layer deposition of transition metals. *Nature Materials* **2003,** *2* (11), 749-754.
50. Hu, X.; Schuster, J.; Schulz, S. E.; Gessner, T., Surface chemistry of copper metal and copper oxide atomic layer deposition from copper (ii) acetylacetonate: a combined first-principles and reactive molecular dynamics study. *Physical Chemistry Chemical Physics* **2015,** *17* (40), 26892-26902.
51. Bobb-Semple, D.; Nardi, K. L.; Draeger, N.; Hausmann, D. M.; Bent, S. F., Area-Selective Atomic Layer Deposition Assisted by Self-Assembled Monolayers: A Comparison of Cu, Co, W, and Ru. *Chemistry of Materials* **2019,** *31* (5), 1635-1645.
52. Niskanen, A.; Rahtu, A.; Sajavaara, T.; Arstila, K.; Ritala, M.; Leskelä, M., Radical-enhanced atomic layer deposition of metallic copper thin films. *Journal of The Electrochemical Society* **2005,** *152* (1), G25-G28.
53. Moon, D.-Y.; Han, D.-S.; Shin, S.-Y.; Park, J.-W.; Kim, B. M.; Kim, J. H., Effects of the substrate temperature on the Cu seed layer formed using atomic layer deposition. *Thin Solid Films* **2011,** *519* (11), 3636-3640.
54. Sasinska, A.; Ritschel, D.; Czympiel, L.; Mathur, S., Metallic Copper Thin Films Grown by Plasma-Enhanced Atomic Layer Deposition of Air Stable Precursors *Advanced Engineering Materials* **2017,** *19* (2), 1600593.
55. Zhang, Y.; Du, L.; Liu, X.; Ding, Y., High growth per cycle thermal atomic layer deposition of Ni films using an electron-rich precursor. *Nanoscale* **2019,** *11* (8), 3484-3488.
56. Kerrigan, M. M.; Klesko, J. P.; Blakeney, K. J.; Winter, C. H., Low Temperature, Selective Atomic Layer Deposition of Nickel Metal Thin Films. *ACS Applied Materials & Interfaces* **2018,** *10* (16), 14200-14208.
57. Yang, H. B.; Hung, S.-F.; Liu, S.; Yuan, K.; Miao, S.; Zhang, L.; Huang, X.; Wang, H.-Y.; Cai, W.; Chen, R.; Gao, J.; Yang, X.; Chen, W.; Huang, Y.; Chen, H. M.; Li, C. M.; Zhang, T.; Liu, B., Atomically dispersed Ni(i) as the active site for electrochemical CO2 reduction. *Nature Energy* **2018,** *3* (2), 140-147.

58. Gong, M.; Wang, D.-Y.; Chen, C.-C.; Hwang, B.-J.; Dai, H., A mini review on nickel-based electrocatalysts for alkaline hydrogen evolution reaction. *Nano Research* **2016,** *9* (1), 28-46.
59. Utriainen, M.; Kröger-Laukkanen, M.; Johansson, L.-S.; Niinistö, L., Studies of metallic thin film growth in an atomic layer epitaxy reactor using M (acac) 2 (M= Ni, Cu, Pt) precursors. *Applied Surface Science* **2000,** *157* (3), 151-158.
60. Wang, G.; Peng, X.; Yu, L.; Wan, G.; Lin, S.; Qin, Y., Enhanced microwave absorption of ZnO coated with Ni nanoparticles produced by atomic layer deposition. *Journal of Materials Chemistry A* **2015,** *3* (6), 2734-2740.
61. Chae, J.; Park, H.-S.; Kang, S.-w., Atomic layer deposition of nickel by the reduction of preformed nickel oxide. *Electrochemical and solid-state letters* **2002,** *5* (6), C64-C66.
62. Do, K.-W.; Yang, C.-M.; Kang, I.-S.; Kim, K.-M.; Back, K.-H.; Cho, H.-I.; Lee, H.-B.; Kong, S.-H.; Hahm, S.-H.; Kwon, D.-H.; Lee, J.-H.; Lee, J.-H., Formation of Low-Resistivity Nickel Silicide with High Temperature Stability from Atomic-Layer-Deposited Nickel Thin Film. *Japanese Journal of Applied Physics* **2006,** *45* (4B), 2975-2979.
63. Sarr, M.; Bahlawane, N.; Arl, D.; Dossot, M.; McRae, E.; Lenoble, D., Tailoring the properties of atomic layer deposited nickel and nickel carbide thin films via chain-length control of the alcohol reducing agents. *The Journal of Physical Chemistry C* **2014,** *118* (40), 23385-23392.
64. Kim, W.-H.; Heo, K.; Lee, Y. K.; Chung, T.-M.; Kim, C. G.; Hong, S.; Heo, J.; Kim, H., Atomic layer deposition of Ni thin films and application to area-selective deposition. *Journal of the Electrochemical Society* **2011,** *158* (1), D1-D5.
65. Knisley, T. J.; Kalutarage, L. C.; Winter, C. H., Precursors and chemistry for the atomic layer deposition of metallic first row transition metal films. *Coordination Chemistry Reviews* **2013,** *257* (23), 3222-3231.
66. Lee, H.-B.-R.; Bang, S.-H.; Kim, W.-H.; Gu, G. H.; Lee, Y. K.; Chung, T.-M.; Kim, C. G.; Park, C. G.; Kim, H., Plasma-Enhanced Atomic Layer Deposition of Ni. *Japanese Journal of Applied Physics* **2010,** *49* (5), 05FA11.
67. Kim, J.-M.; Lee, H.-B.-R.; Lansalot, C.; Dussarrat, C.; Gatineau, J.; Kim, H., Plasma-Enhanced Atomic Layer Deposition of Cobalt Using Cyclopentadienyl Isopropyl Acetamidinato-Cobalt as a Precursor. *Japanese Journal of Applied Physics* **2010,** *49* (5), 05FA10.
68. Delarosa, M. J.; Lu, T.-M.; Kumar, A., Atomic layer deposition of cobalt from cobalt metallorganic compounds. Google Patents: 2003.
69. Kim, K.; Lee, K.; Han, S.; Jeong, W.; Jeon, H., Characteristics of cobalt thin films deposited by remote plasma ALD method with dicobalt octacarbonyl. *Journal of The Electrochemical Society* **2007,** *154* (3), H177-H181.
70. Lee, K.; Kim, K.; Park, T.; Jeon, H.; Lee, Y.; Kim, J.; Yeom, S., Characteristics of Ti-capped Co films deposited by a remote plasma ALD method using cyclopentadienylcobalt dicarbonyl. *Journal of The Electrochemical Society* **2007,** *154* (10), H899-H903.
71. Lee, H. B. R.; Park, Y. J.; Baik, S.; Kim, H., Initial Stage Growth during Plasma-Enhanced Atomic Layer Deposition of Cobalt. *Chemical Vapor Deposition* **2012,** *18* (1-3), 41-45.
72. Park, J.; Kim, D.; Yoon, J.; Lansalot, C.; Gatineau, J.; Chevrel, H.; Kim, H., Plasma-enhanced atomic layer deposition of Co using Co (MeCp) 2 precursor. *Journal of Energy Chemistry* **2013,** *22* (3), 403-407.
73. Zhu, B.; Ding, Z.-J.; Wu, X.; Liu, W.-J.; Zhang, D. W.; Ding, S.-J., Plasma-Enhanced Atomic Layer Deposition of Cobalt Films Using Co(EtCp)2 as a Metal Precursor. *Nanoscale Research Letters* **2019,** *14* (1), 76.
74. Pedreira, O. V.; Croes, K.; Leśniewska, A.; Wu, C.; Veen, M. H. v. d.; Messemaeker, J. d.; Vandersmissen, K.; Jourdan, N.; Wen, L. G.; Adelmann, C.; Briggs, B.; Gonzalez, V. V.; Bömmels, J.; Tőkei, Z. In *Reliability study on cobalt and ruthenium as alternative metals for advanced interconnects*, 2017 IEEE International Reliability Physics Symposium (IRPS), 2-6 April 2017; 2017; pp 6B-2.1-6B-2.8.

75. Qiu, X.; Burda, C., Chemically synthesized nitrogen-doped metal oxide nanoparticles. *Chemical Physics* **2007,** *339* (1), 1-10.
76. Di Valentin, C.; Pacchioni, G.; Selloni, A., Theory of Carbon Doping of Titanium Dioxide. *Chemistry of Materials* **2005,** *17* (26), 6656-6665.
77. Kalutarage, L. C.; Martin, P. D.; Heeg, M. J.; Winter, C. H., Volatile and thermally stable mid to late transition metal complexes containing α-imino alkoxide ligands, a new strongly reducing coreagent, and thermal atomic layer deposition of Ni, Co, Fe, and Cr metal films. *Journal of the American Chemical Society* **2013,** *135* (34), 12588-12591.
78. Juppo, M.; Vehkamäki, M.; Ritala, M.; Leskelä, M., Deposition of molybdenum thin films by an alternate supply of MoCl 5 and Zn. *Journal of Vacuum Science & Technology A: Vacuum, Surfaces, and Films* **1998,** *16* (5), 2845-2850.
79. Klesko, J. P.; Thrush, C. M.; Winter, C. H., Thermal atomic layer deposition of titanium films using titanium tetrachloride and 2-methyl-1, 4-bis (trimethylsilyl)-2, 5-cyclohexadiene or 1, 4-bis (trimethylsilyl)-1, 4-dihydropyrazine. *Chemistry of Materials* **2015,** *27* (14), 4918-4921.
80. Bernal Ramos, K.; Saly, M. J.; Chabal, Y. J., Precursor design and reaction mechanisms for the atomic layer deposition of metal films. *Coordination Chemistry Reviews* **2013,** *257* (23), 3271-3281.
81. Zhao, F.; Gong, M.; Cao, K.; Zhang, Y.; Li, J.; Chen, R., Atomic Layer Deposition of Ni on Cu Nanoparticles for Methanol Synthesis from CO2 Hydrogenation. *ChemCatChem* **2017,** *9* (19), 3772-3778.
82. Moon, D.-Y.; Han, D.-S.; Park, J.-H.; Shin, S.-Y.; Park, J.-W.; Kim, B. M.; Cho, J. Y., Plasma-enhanced atomic layer deposition of Cu–Mn films with formation of a MnSixOy barrier layer. *Thin solid films* **2012,** *521*, 146-149.
83. Espejo, A. P.; Zierold, R.; Gooth, J.; Dendooven, J.; Detavernier, C.; Escrig, J.; Nielsch, K., Magnetic and electrical characterization of nickel-rich NiFe thin films synthesized by atomic layer deposition and subsequent thermal reduction. *Nanotechnology* **2016,** *27* (34), 345707.
84. Gould, T. D.; Montemore, M. M.; Lubers, A. M.; Ellis, L. D.; Weimer, A. W.; Falconer, J. L.; Medlin, J. W., Enhanced dry reforming of methane on Ni and Ni-Pt catalysts synthesized by atomic layer deposition. *Applied Catalysis A: General* **2015,** *492*, 107-116.
85. Elko-Hansen, T. D.-M.; Dolocan, A.; Ekerdt, J. G., Atomic Interdiffusion and Diffusive Stabilization of Cobalt by Copper During Atomic Layer Deposition from Bis (N-tert-butyl-N'-ethylpropionamidinato) Cobalt (II). *The journal of physical chemistry letters* **2014,** *5* (7), 1091-1095.
86. Park, J.-H.; Han, D.-S.; Kang, Y.-J.; Shin, S.-R.; Park, J.-W., Self-forming Al oxide barrier for nanoscale Cu interconnects created by hybrid atomic layer deposition of Cu–Al alloy. *Journal of Vacuum Science & Technology A* **2014,** *32* (1), 01A131.
87. Sheng, J.; Lee, J.-H.; Choi, W.-H.; Hong, T.; Kim, M.; Park, J.-S., Review Article: Atomic layer deposition for oxide semiconductor thin film transistors: Advances in research and development. **2018,** *36* (6), 060801.
88. Kim, H., Atomic layer deposition of metal and nitride thin films: Current research efforts and applications for semiconductor device processing. **2003,** *21* (6), 2231-2261.
89. Leskelä, M.; Ritala, M., Atomic Layer Deposition Chemistry: Recent Developments and Future Challenges. **2003,** *42* (45), 5548-5554.
90. Kim, H.; McIntyre, P. C., Atomic layer deposition of ultrathin metal-oxide films for nano-scale device applications. *Journal of the Korean Physical Society* **2006,** *48* (1), 5-17.
91. Hu, J.; Wong, H.-S. P., Effect of annealing ambient and temperature on the electrical characteristics of atomic layer deposition Al2O3/In0.53Ga0.47As metal-oxide-semiconductor capacitors and MOSFETs. **2012,** *111* (4), 044105.
92. Ganesh, K. J.; Darbal, A. D.; Rajasekhara, S.; Rohrer, G. S.; Barmak, K.; Ferreira, P. J., Effect of downscaling nano-copper interconnects on the microstructure revealed by high resolution TEM-orientation-mapping. *Nanotechnology* **2012,** *23* (13), 135702.
93. Perrine, K. A.; Teplyakov, A. V., Reactivity of selectively terminated single crystal silicon surfaces. *Chemical Society Reviews* **2010,** *39* (8), 3256-3274.

94. Yang, Z.; Chen, B.; Chen, W.; Qu, Y.; Zhou, F.; Zhao, C.; Xu, Q.; Zhang, Q.; Duan, X.; Wu, Y., Directly transforming copper (I) oxide bulk into isolated single-atom copper sites catalyst through gas-transport approach. *Nature Communications* **2019,** *10* (1), 3734.

Figures

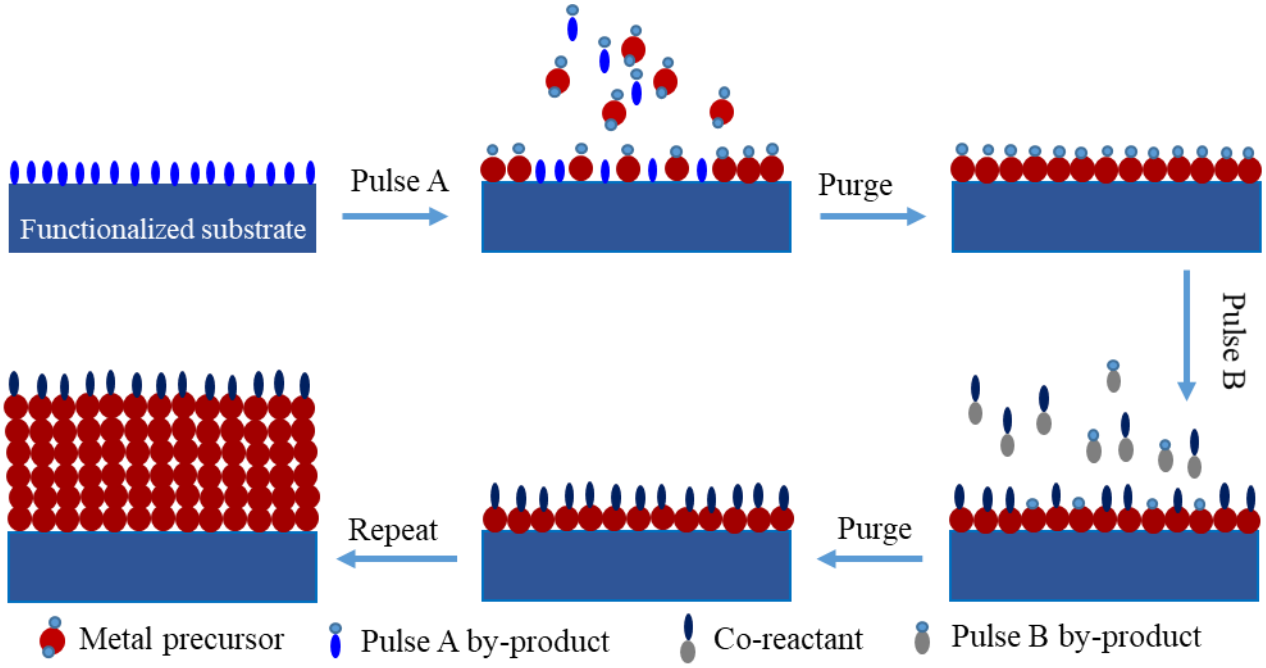

Scheme 1. Schematic illustration of atomic layer deposition of metals.

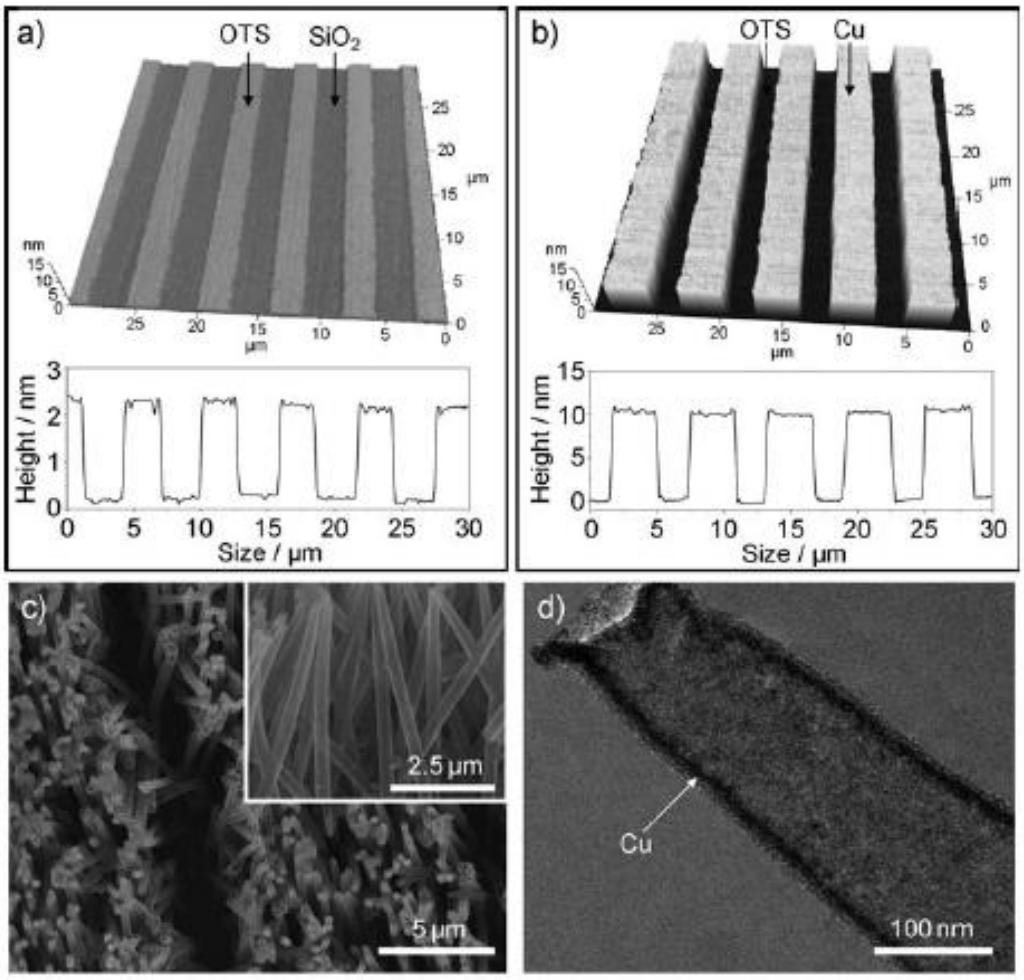

Figure 1. The demonstration of selective and templated deposition of Cu; (a) atomic force microscopy (AFM) image of OTS-SAMs patterned SiO_2 substrate (b) selective deposition of Cu on the OTS patterned surface, (c) SEM images of Cu nanotubes produced using nanoporous polymer membrane as template and (d) HR-TEM images of a Cu nanotube. Reproduced from ref. [15] with permission from Wiley Online Libraries.

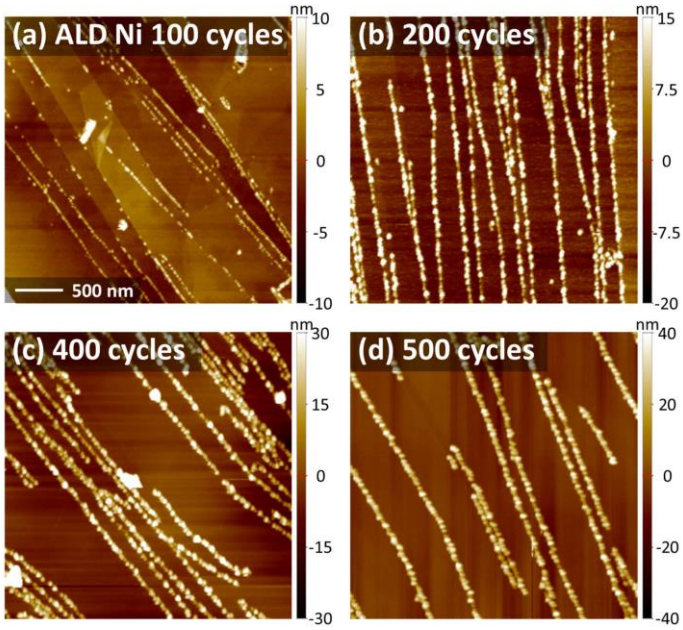

Figure 2. Selective deposition of Ni nanowires across the edges of pyrolytic graphene, after (a) 100 cycles, (b) 200 cycles, (c) 400 cycles, (d) 500 cycles. Reproduced from Ref.[16] with permission from IOP Science.

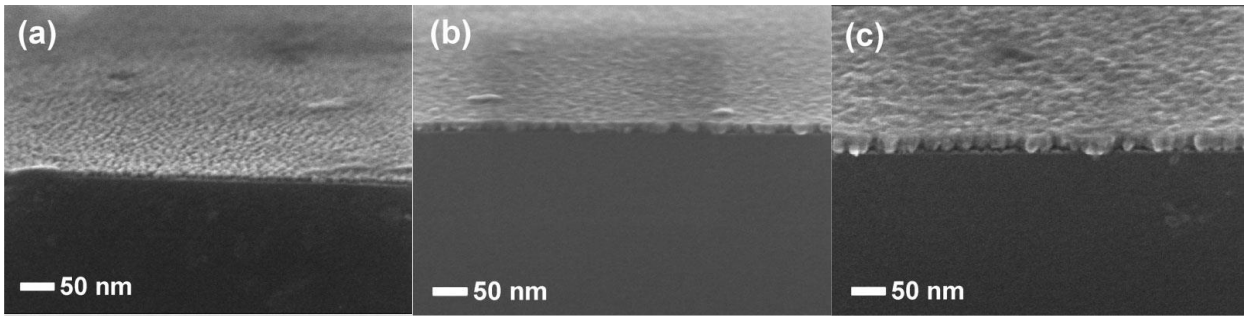

Figure 3. The surface morphology of PE-ALD Co film after a)100, b) 300, and c) 500 cycles. The surface morphology became smooth and more continuous as the number of deposition cycles were increased from 100 to 500 cycles. Reproduced from Ref.[71]with permission from Wiley Online Library.

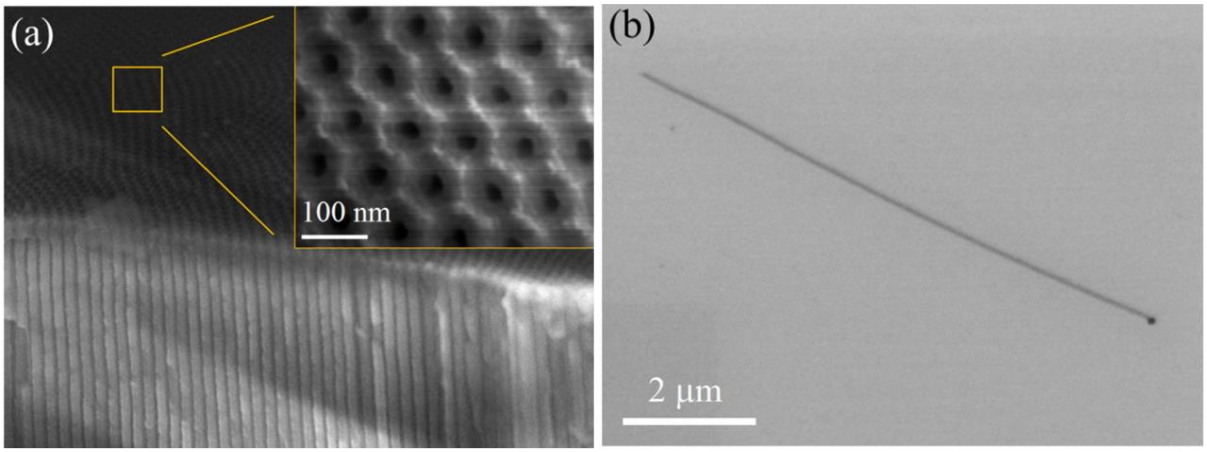

Figure 4. (a) SEM image of ALD $Ni_{83}Fe_{17}$ nanotubes embedded in a nanoporous alumina membrane, (b) SEM image of an isolated nanotube with an external diameter of about 70 nm and a length of 8.7 µm. Reproduced from Ref.[83] with permission from IOP Science.

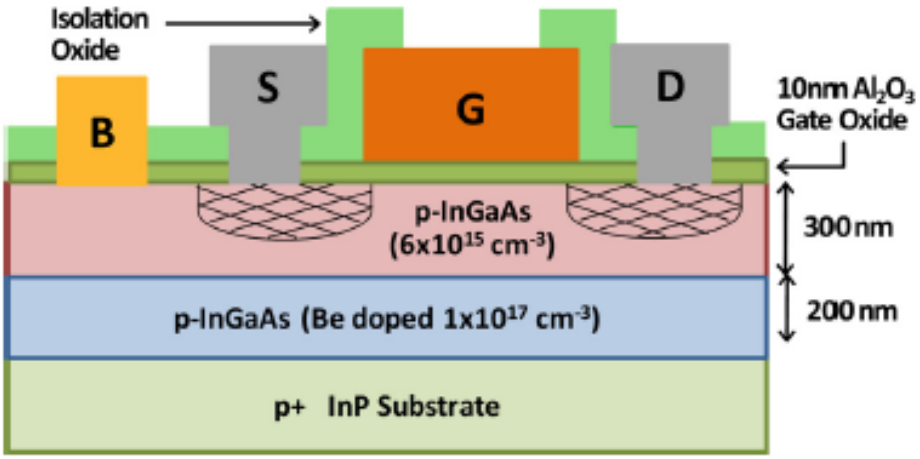

Figure 5. A schematic illustration of InGaAs MOSFET with a 10 nm ALD Al_2O_3 gate oxide.[91] Reproduced from Ref.[91] with permission from AIP publishing LLC.

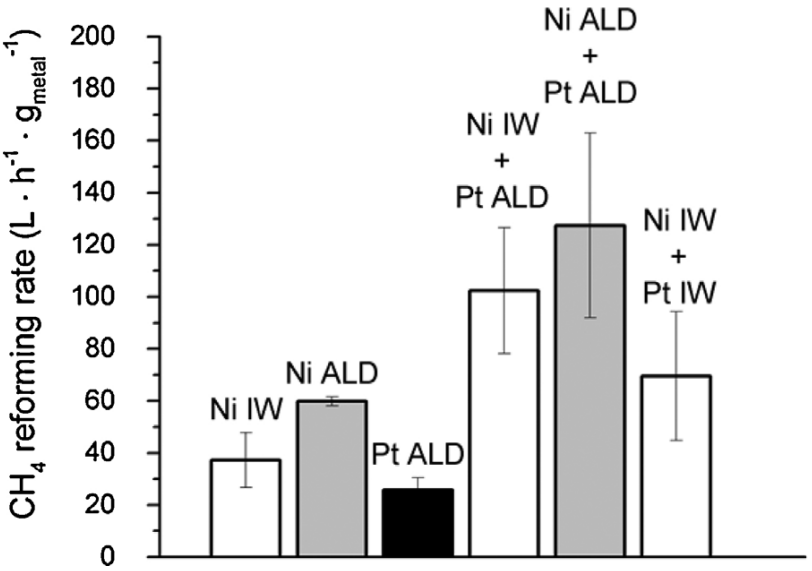

Figure 6. Dry reforming of methane at 600 ºC using Ni-Pt core shell nanoparticles. Consistently higher reforming rate was achieved with the bi-metal particles as compared to either pure Ni or Pt. The reforming rate obtained with the ALD core-shell particles was twice as fast compared to that obtained with particles prepared through the incipient wet impregnation (IW) method. Reproduced from Ref.[84] with permission from Elsevier.